SCEP1 and SCEP2 are two new components of the synaptonemal complex central element

Nathalie Vrielynck, Marion Peuch, Stéphanie Durand, Qichao Lian, Aurélie Chambon, Aurélie Hurel, Julie Guérin, Raphaël Guérois, Raphaël Mercier, Mathilde Grelon, et al.

nature plants

Article

https://doi.org/10.1038/s41477-023-01558-y

SCEP1 and SCEP2 are two new components of the synaptonemal complex central element

Received: 16 June 2023

Accepted: 28 September 2023

Published online: 16 November 2023

Check for updates

Nathalie Vrielynck[1,5], Marion Peuch[1,5], Stéphanie Durand[2], Qichao Lian[2], Aurélie Chambon[1], Aurélie Hurel[1], Julie Guérin[1], Raphaël Guérois[3], Raphaël Mercier[2], Mathilde Grelon[1] ✉ & Christine Mézard[1,4] ✉

The synaptonemal complex (SC) is a proteinaceous structure that forms between homologous chromosomes during meiosis prophase. The SC is widely conserved across species, but its structure and roles during meiotic recombination are still debated. While the SC central region is made up of transverse filaments and central element proteins in mammals and fungi, few central element proteins have been identified in other species. Here we report the identification of two coiled-coil proteins, SCEP1 and SCEP2, that form a complex and localize at the centre of the *Arabidopsis thaliana* SC. In *scep1* and *scep2* mutants, chromosomes are aligned but not synapsed (the ZYP1 transverse filament protein is not loaded), crossovers are increased compared with the wild type, interference is lost and heterochiasmy is strongly reduced. We thus report the identification of two plant SC central elements, and homologues of these are found in all major angiosperm clades.

In meiosis, haploid cells are formed by two successive rounds of cell divisions occurring after one step of DNA replication. In many species, crossovers (COs) (exchanges of genetic material produced by recombination between homologous chromosomes) are essential for the correct segregation of chromosomes during the first meiotic division. Concomitant with the molecular events forming the COs during prophase of the first meiotic division, each pair of homologous chromosomes becomes tightly synapsed to each other along their entire length by a proteinaceous structure known as the synaptonemal complex (SC)[1]. Cytological observations performed in many species have described the SC as a zipper-like tripartite structure with two rods forming the lateral elements (LEs), one at the base of each pair of sister chromatids, and a multilayered central region[2]. The SC central region is composed of transverse filaments (TFs) and, in many species, central element (CE) proteins. TFs are formed by dimers of long coiled-coil proteins (ZYP1A and ZYP1B in *Arabidopsis thaliana*[3–5]; Zip1 in *Saccharomyces cerevisiae*[6]; SCYP1 in mice[7]; SYP-1, SYP-5 and SYP6 in *Caenorhabditis elegans*[8–10]; and C(3)G in *Drosophila*[11]) with their amino-terminal globular domains arranged head-to-head in the centre of the SC and their carboxy termini at the LEs[12]. Twelve different CE proteins have been identified: five in mice (SYCE1, SYCE2, SYCE3, TEX12 and SIX6OS1)[13–16], three in *C. elegans* (SYP-2, SYP-3 and SYP-4)[17–19], two in *S. cerevisiae* (Ecm11 and Gmc2)[20] and two in *Drosophila* (CONA and Corolla)[21,22]. No significant sequence similarity between CE proteins across species has been identified, but they often display either a long α-helix or a coiled-coiled structure[23]. CE proteins have been shown to promote the polymerization, stabilization and/or reorganization of TFs[24]. The absence of CE proteins has different consequences, depending on the model species. In mice, *C. elegans* or *Drosophila*, the loss of any CE protein leads to severe meiotic defects and sterility, impaired synapsis and the absence of CO formation[13–19,21,22]. In *S. cerevisiae*, in the absence of Ecm11 or Gmc2, sporulation is delayed, spore viability is only slightly reduced and the TF protein Zip1 exhibits a dotty pattern, but COs are formed and found to be increased on certain chromosomes[20].

CE proteins associate in subcomplexes through their α-helix or coiled-coil regions, and the complexes self-assemble to form higher-order structures with different roles within the SC. For example, in mice, the SYCE3 protein self-assembles and remodels TF organization[25]. SYCE3 also interacts with the two CE subcomplexes SIX60S1–SYCE1 and TEX12–SYCE2, providing a means for their recruitment

[1]Université Paris-Saclay, INRAE, AgroParisTech, Institut Jean-Pierre Bourgin, Versailles, France. [2]Department of Chromosome Biology, Max Planck Institute for Plant Breeding Research, Cologne, Germany. [3]Université Paris-Saclay, CEA, CNRS, Institute for Integrative Biology of the Cell, Gif-sur-Yvette, France. [4]Université Paris-Saclay, INRAE, AgroParisTech, CNRS, Institut Jean-Pierre Bourgin, Versailles, France. [5]These authors contributed equally: Nathalie Vrielynck, Marion Peuch. ✉e-mail: Mathilde.grelon@inrae.fr; Christine.mezard@inrae.fr

on the SC[25]. Biochemical and biophysical analyses suggest that each high-affinity subcomplex formed by SYCE3–SYCP1, TEX12–SYCE2 and SYCE1–SIX6OS1 assembles into higher structures (self- or hetero-assembled lattices and/or fibres) and that the three subcomplexes transiently interact by low-affinity connections that are dynamic during SC formation[25]. The mammalian TEX12–SYCE2 complex exhibits structural and functional similarities to the yeast Ecm11–Gmc2 protein complex[26]. Both Ecm11 and TEX12 interact with the ZMM protein Zip4 in yeast and the mouse Zip4 homologue TEX11, which belong to the ZMM (Zip1-4, Msh4-5, Mer3 and Spo16) group of proteins, which control the formation of most COs. Moreover, AlphaFold2 predicts that Ecm1 and Gmc2 form a tetramer[26] very similar to the crystal structure obtained for the TEX12–SYCE2 tetramer[27]. In *C. elegans*, the localization of each SYP protein is dependent on the presence of all the other SYPs, confirming that they all participate in a common structure[8,17–19]. SYP-3 and SYP-4 form a complex with the SYP-3 C terminus located close to the LE and the SYP-4 N terminus in the centre of the SC. The small SYP-2 protein interacts with the SYP-1 N terminus and localizes at the SC centre[28]. The two *Drosophila* CE proteins CONA and Corolla also interact with each other, with CONA localizing close to the N terminus of the C(3)G TF[22,29]. The localizations of CONA, Corolla and C(3)G depend on each other. Considering the crucial role of CE proteins in the structure and functions of the SC in various species, it is intriguing that no CE proteins have been identified in plants, and the question remains as to whether CE proteins exist outside metazoa and fungi.

To identify new meiotic players in *A. thaliana*, we set up a screen based on transcriptomic data. Here we describe the identification of two small coiled-coil proteins, SCEP1 and SCEP2. Orthologues of these two proteins can be detected in all major angiosperm clades as well as in more distant species such as ferns (within the Tracheophytes clade) but not in other species such as mosses or algae. SCEP1 and SCEP2 interact with each other, colocalize with ZYP1 in the central region of the SC and are mutually interdependent for their loading on the SC. When they are mutated, TFs are not formed, synapsis does not occur and COs are increased. Altogether, these data suggest that SCEP1 and SCEP2 belong to the CE of the SC and participate in the control of CO formation.

Results

Identification of SCEP1 and SCEP2

From the analysis of the transcriptomic data published in ref. 30, we noticed that 23 of the 28 genes known to have a specific role in *A. thaliana* meiosis (*ASY1*, *ASY3*, *ASY4*, *DFO*, *DMC1*, *DUET*, *HEI10*, *JASON*, *MER3*, *MSH4*, *MSH5*, *MTOPVIB*, *OSD1*, *PCH2*, *PHS1*, *PRD1*, *PRD2*, *PRD3*, *PTD*, *REC8*, *SCHOC1*, *SDS*, *SPO11-1*, *SPO11-2*, *SWI1*, *ZYP1A*, *ZYP1B* and *ZIP4*) had an expression peak at a stage where flower buds have a size of about 0.5 mm (Fig. 1a and Supplementary Table 1). This size marks the stage at which male meiosis takes place within the flower buds[31]. We analysed the expression profiles of the full set of *A. thaliana* genes in flowers and selected 80 genes that presented expression profiles similar to those of known meiotic genes (Methods). Among them, we selected the gene AT1G33500, hereafter called *SCEP1*, for further characterization.

Using CRISPR–Cas9 with three guide RNAs (gRNAs) targeting three different sites in *SCEP1* (Fig. 1 and Extended Data Fig. 1), we identified six independent mutations in the Columbia accession with various insertions/deletions leading to a frameshift at several positions: after the first 20 amino acids for *scep1-1* and *scep1-2*, after the first 55 amino acids for *scep1-3*, and after the first 114 amino acids for *scep1-4* and *scep1-5*. The mutant *scep1-6* had a deletion of 96 amino acids between amino acids 20 and 116. We also obtained a mutation in the Landsberg *erecta* accession (*scep1-7*) with a premature stop codon at the same position as in *scep1-1* (Extended Data Fig. 1).

We explored chromosome behaviour during male meiosis in the *scep1* mutant series. In chromosome spreads stained with 4′,6-diamidino-2-phénylindole (DAPI), 10% to 25% of the cells at metaphase I exhibited one or two pairs of univalents instead of the five pairs of bivalents observed in 100% of the wild-type meiocytes (Fig. 1b,c). As an expected consequence of this defect in bivalent formation, unequal segregation of chromosomes was observed at anaphase I–metaphase II–anaphase II with a 6:4 chromosome distribution in 7% to 20% of the cells (Fig. 1b and Supplementary Fig. 1). Thus, in the absence of SCEP1, there is a failure to form at least one CO per bivalent. At earlier prophase stages, *scep1* leptotenes were not different from wild-type leptotenes. At the pachytene stage, in wild-type meiosis, homologous chromosomes are fully synapsed and appear as fluffy structures in which the two homologous chromosomes are paired and hardly distinguishable from each other. However, in *scep1* mutant cells, we observed that large chromosome regions were aligned and remained distinguishable (unsynapsed) (Supplementary Fig. 1), and typical pachytene stages were never observed ($n = 50$).

The transcriptomic data from ref. 30 predicted two isoforms of SCEP1 differing in the 3′-terminal part of the proteins. After sequencing the 3′ ends of complementary DNAs, we found only the short form corresponding to a 254-amino-acid protein (Methods and Extended Data Fig. 1). SCEP1's structure was analysed using AlphaFold2 (ref. 32). Five separate structure predictions were performed and showed high levels of similarity with each other. SCEP1 was predicted with a high probability (76% of residues have predicted local distance difference test (pLDDT) values above 85) to be a small coiled-coil protein with two long α-helices; the short region between the two α-helices around the middle of the protein (amino acids 135 to 144) had a low pLDDT value, indicating that the protein might not fold as depicted in Fig. 1e.

Using the ColabFold notebook[33], we explored the predicted structure of proteins with a meiotic-like profile of expression (Fig. 1a). AT3G28370, referred to as SCEP2, was predicted to have a very similar structure to SCEP1: a small coiled-coil protein with two α-helices separated by a small unstructured region (residues 136–153). As for SCEP1, the predicted C-terminal part of SCEP2 was uncertain. After sequencing the cDNAs, we found two isoforms that differ in the last 45 amino acids with a long (262 amino acids) and a short (227 amino acids) protein. This variable C terminus is poorly predicted by AlphaFold2 (Fig. 1e and Extended Data Fig. 1d–f). We examined the behaviour of the chromosomes in the line N663933 (*scep2-1*), where the transfer DNA (T-DNA) was inserted in the second exon of the gene (Fig. 1d and Extended Data Fig. 1d,f). The meiotic defect observed was similar to the one observed in cells with the *scep1* alleles: around 10% of metaphase I had a defect in bivalent formation with one pair of univalents (6/54), 5% of metaphase II–anaphase II had a 6:4 chromosome distribution (3/83) and no true synapsis in prophase I was observed (Fig. 1b,c and Supplementary Fig. 1).

We measured the fertility of *scep1-1* and *scep2-1* mutant plants by counting the number of seeds per silique. We found that the fertility was slightly lower than in the wild-type plants, with 58.9 and 57.2 seeds per silique in *scep1-1* ($P = 4 \times 10^{-4}$) and *scep2-1* ($P < 10^{-5}$), respectively, compared with 63.3 in the wild type (Fig. 1f and Supplementary Table 8).

In conclusion, we identified two small coiled-coil proteins, SCEP1 (AT1G33500) and SCEP2 (AT3G28370), which are required for efficient formation of chromosome bivalents at metaphase I and for full fertility.

SCEP1 and SCEP2 are required to form TFs

DAPI staining of chromosomes suggested that synapsis was defective in *scep1* and *scep2* mutants. We wondered whether the ZYP1 proteins that form the TF structure of the SC were normally loaded in *scep1* and *scep2* mutants. We performed immunolocalization of the axis protein ASY1 together with ZYP1. In wild-type pachytene cells, the ZYP1 signal forms a continuous line along the synapsed chromosomes, while the ASY1 labelling is faint due to its partial removal from the chromosome axes[31,34] (Fig. 2a). In *scep1-1* and *scep2-1*, however, there was no ZYP1 signal, and the ASY1 labelling did not weaken in zygotene-like or pachytene-like cells (Fig. 2a). Moreover, the two axes appeared as two

https://doi.org/10.1038/s41477-023-01558-y

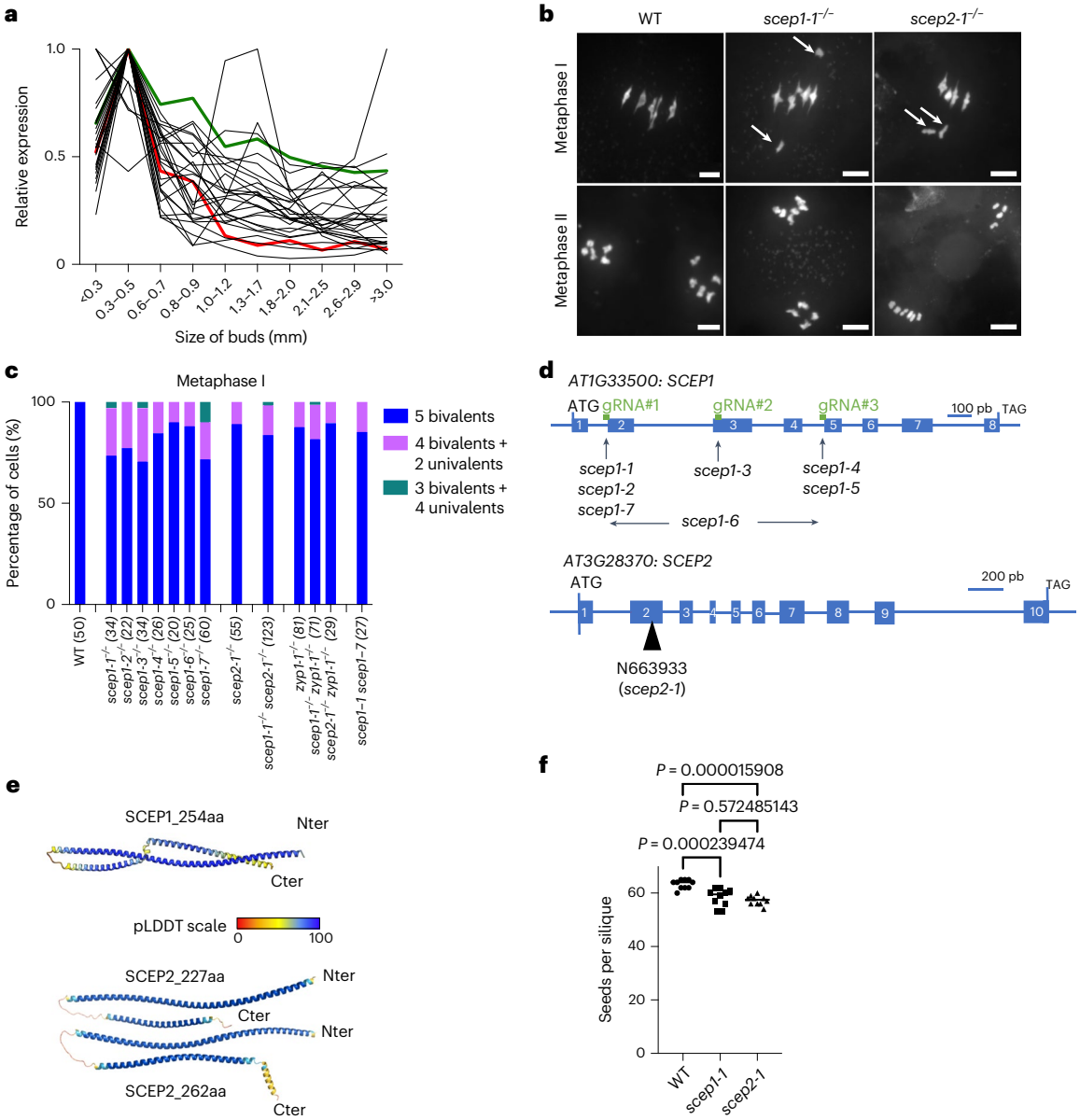

Fig. 1 | Identification and characterization of SCEP1 and SCEP2. a, Expression profiles of 28 known meiotic genes (Supplementary Table 1) in buds of various sizes including *SCEP1* in red and *SCEP2* in green. **b**, DAPI staining of chromosomes in male meiosis at metaphase I or metaphase II in the wild type (WT), *scep1-1* and *scep2-1*. The white arrows indicate univalents. Scale bars, 5 µm. **c**, Quantification of univalents at metaphase I. The number of cells is shown in parentheses. **d**, Structures obtained from TAIR showing the introns and exons of the *SCEP1* and *SCEP2* genes. The position of the gRNA (green) used for CRISPR–Cas9 in *SCEP1* are placed above the gene structure, and the positions of the mutant alleles are indicated below the gene structure. The position of the T-DNA insertion in *SCEP2* is indicated below the gene structure. **e**, Predicted structures of SCEP1 and SCEP2 from AlphaFold2 coloured by per-residue pLDDT. High pLDDT values indicate strong confidence in the predicted structure, and low values indicate low confidence. The SCEP1 and SCEP2 protein sequences were deduced after sequencing cDNAs. Two different putative proteins were found for SCEP2 that differ by the last 50 amino acids (Methods and Extended Data Fig. 1) Nter, N terminus; Cter, C terminus. **f**, Mean number of seeds per silique. The numbers of plants and siliques are shown in Supplementary Table 8. Tukey's multiple comparison test was used to determine significance.

parallel lines instead of a weak single line as in the wild type, suggesting that chromosome pairing occurs but synapsis does not.

Using ASY1 and REC8 immunolocalization and stimulated emission depletion (STED) microscopy on wild-type pachytene cells, we were able to visualize the two parallel LE axes along the synapsed chromosomes, at a distance of 175 ± 23 nm (Fig. 2b,c). In *scep1-1* and *scep2-1*, the two axes decorated by REC8 and ASY1 were also aligned but at a mean distance of 285 ± 68 nm, which is 1.6 times the distance observed in the wild type (Fig. 2b,c). In addition, the distance between the two axes has a higher variability in *scep1* and *scep2* mutants than in the wild type (Fig. 2c). Thus, in the absence of SCEP1 and SCEP2, pairing occurs, but ZYP1 proteins are not loaded on the SC, and synapsis does not take place.

SCEP1 and SCEP2 localize in the middle region of the SC

We raised antibodies against SCEP1 and SCEP2 and analysed their localization on chromosome spreads during male meiosis together with ASY1 and/or ZYP1. In *scep1-1* cells, no signal was observed with the SCEP1 antibody in male meiocytes. Likewise, no signal was seen with the SCEP2 antibody in *scep2-1* meiocytes (Extended Data Fig. 2).

https://doi.org/10.1038/s41477-023-01558-y

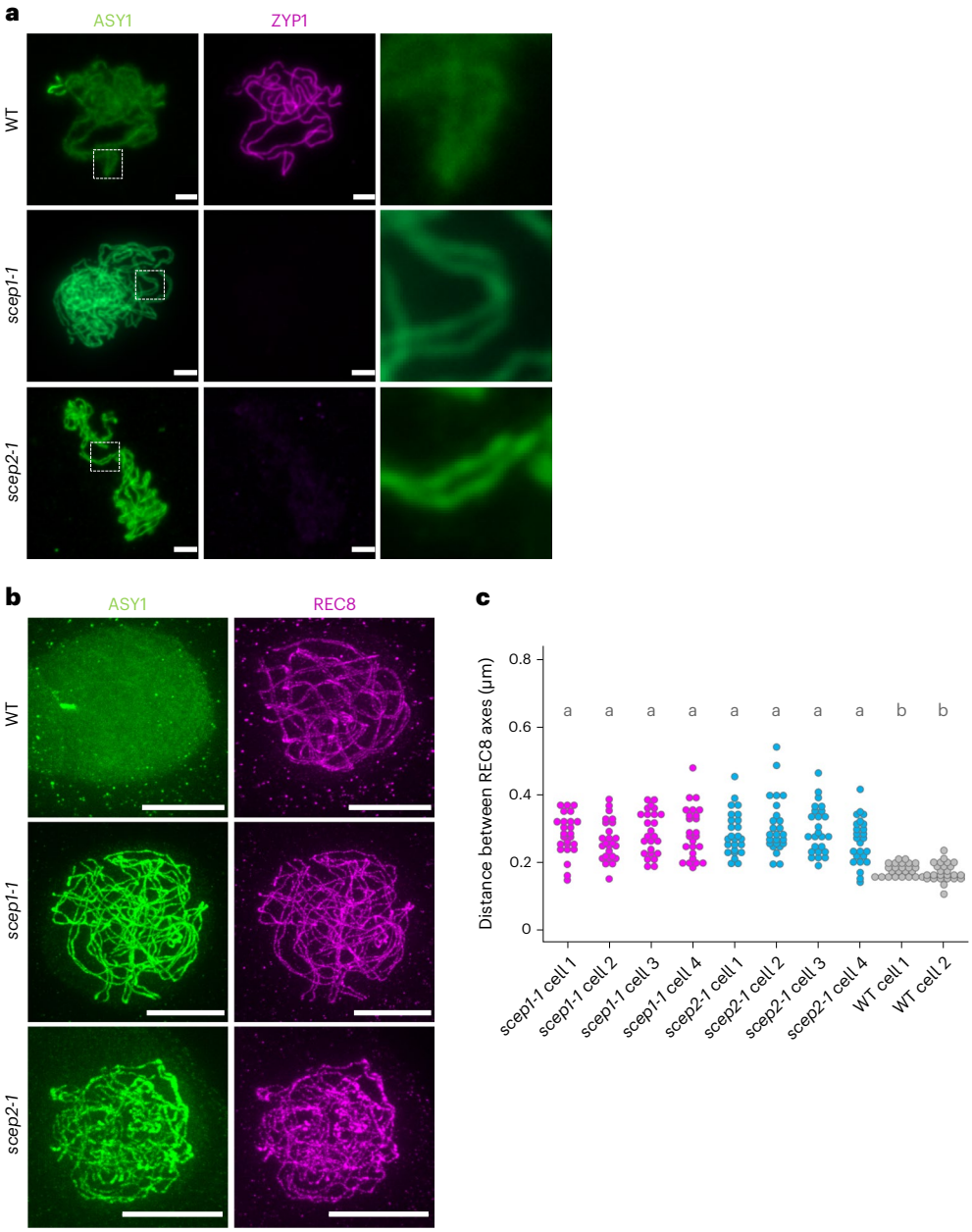

Fig. 2 | ZYP1 is not loaded in *scep1* and *scep2* mutants. a, Immunolocalization of ZYP1 and ASY1 in WT, *scep1-1* and *scep2-1* male meiocytes (standard-resolution microscopy). Scale bars, 2 µm. **b**, Immunolocalization of ASY1 (green) and REC8 (magenta) in WT, *scep1-1* and *scep2-1* male meiocytes analysed with STED microscopy. Scale bars, 5 µm. **c**, Comparison of lateral distances between REC8 axes in WT, *scep1-1* and *scep2-1* cells. The *P* value for the difference between groups a and b was determined using Tukey's honestly significant difference test: $P < 10^{-4}$.

In wild-type cells, both the SCEP1 and the SCEP2 signals were first seen at the zygotene stage on synapsed chromosomal regions identified by faint ASY1 labelling and bright ZYP1 signals, with which they perfectly colocalized (Fig. 3). We did not observe one of the three proteins SCEP1, SCEP2 or ZYP1 being loaded before the others. At the pachytene stage, SCEP1 and SCEP2 decorated the full length of synapsed chromosomes and perfectly colocalized with the ZYP1 signal (Fig. 3b–d). Using STED microscopy, we compared the localization of SCEP1 and SCEP2 with that of ZYP1 and REC8. SCEP2 formed a single line lying between the two parallel lines formed by REC8 (Fig. 4a). In *Arabidopsis*, as in other species, the TF proteins were shown to have their globular C termini associated with the lateral axes of the homologues and the N termini overlapping in the central region of the SC[4,5]. The accurate localization of SCEP2 was further investigated using an antibody raised against the very C-terminal part of ZYP1 that labels the most external part of the TF (Methods). We observed that SCEP2 was localized between the two ZYP1 C terminus signals (Fig. 4b), showing its central localization on the central region of the SC. When REC8 and SCEP1 were co-immunolocalized, SCEP1 localized between the two REC8 lines (Fig. 4c). In some regions the SCEP1 signal was compatible with the formation of a double line between the two REC8 axes, whereas in other places a single line could be seen in the centre of the SC (Fig. 4c). We also observed that when SCEP1 and SCEP2 co-immunolocalized, SCEP2 broadly colocalized with the SCEP1 signal that closely surrounds some portions of the SCEP2 signal (Fig. 4d). When two SCEP1 lines were detected, they were 95 ± 19 nm apart and thus within the two ZYP1 C terminus lines, which were 170 nm apart (Fig. 4e). We can therefore conclude that SCEP1 and SCEP2 both localize in the middle of the central region of the SC.

https://doi.org/10.1038/s41477-023-01558-y

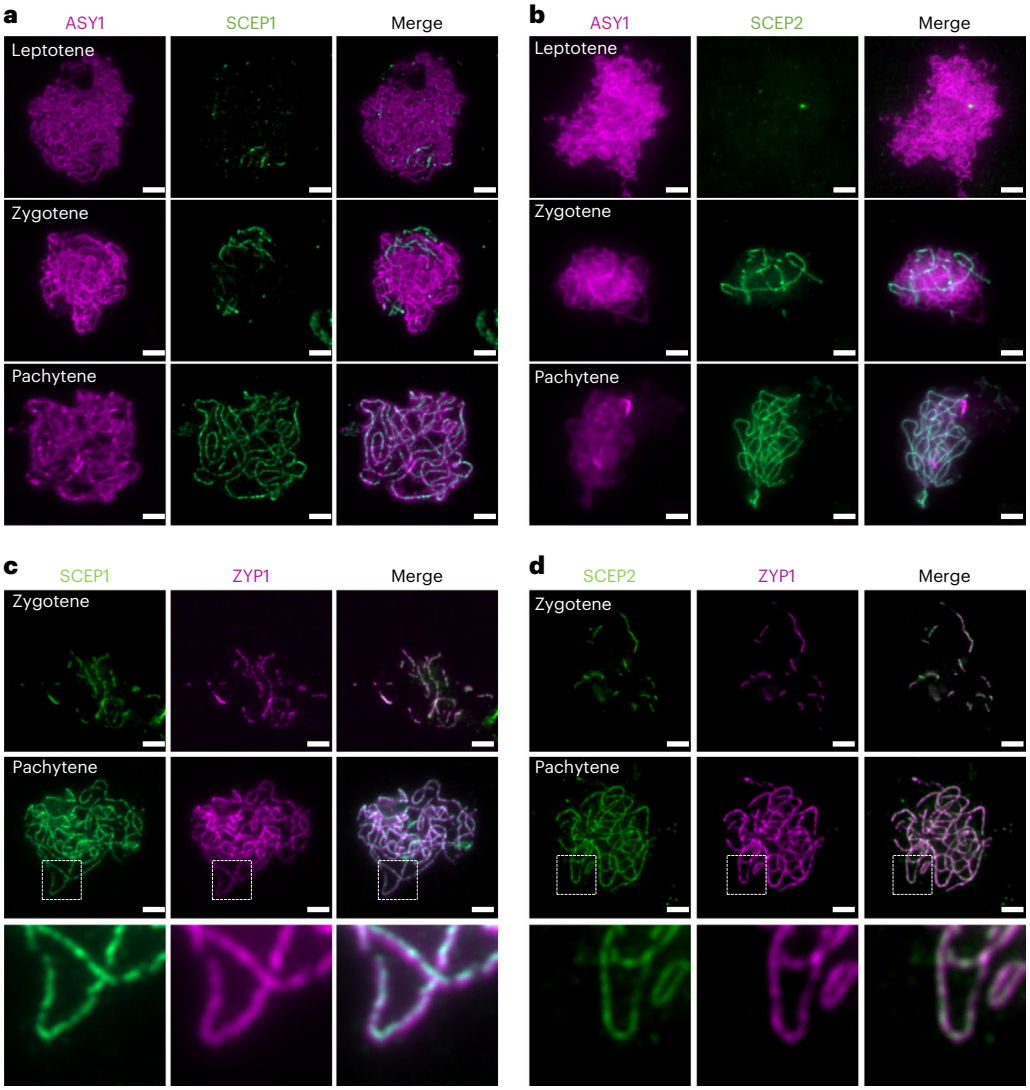

Fig. 3 | SCEP1 and SCEP2 are loaded on the SC central region. **a**, Immunolocalization of ASY1 (magenta) and SCEP1 (green) in WT male meiocytes analysed by standard-resolution microscopy. The leptotene (top), zygotene (middle) and pachytene (bottom) stages are shown. Scale bars, 2 µm. **b**, Immunolocalization of ASY1 (magenta) and SCEP2 (green) in WT male meiocytes analysed by standard-resolution microscopy. The leptotene (top), zygotene (middle) and pachytene (bottom) stages are shown. Scale bars, 2 µm. **c**, Immunolocalization of ZYP1s (magenta) and SCEP1 (green) in WT male meiocytes at the zygotene (top) or pachytene (middle) stage analysed by standard-resolution microscopy. The bottom row shows an enlargement of the area in the dashed box. Scale bars, 2 µm. **d**, Immunolocalization of ZYP1s (magenta) and SCEP2 (green) in WT male meiocytes at the zygotene (top) or pachytene (middle) stage analysed by standard-resolution microscopy. The bottom row shows an enlargement of the area in the dashed box. Scale bars, 2 µm.

SCEP1, SCEP2 and ZYP1s are needed to form the SC

As reported above, ZYP1 proteins were not detected between the two LEs in the *scep1-1* and *scep2-1* mutants (Fig. 2a). We then wondered whether SCEP1 and SCEP2 could be detected in *zyp1* mutants. We immunolocalized SCEP1 in *scep2-1* meiocytes and in the null *zyp1-1* line[4] and did not obtain any signal (Fig. 5a; $n = 11$ and $n = 21$, respectively). Reciprocally, SCEP2 was also undetectable in both *scep1-1* and *zyp1-1* mutants (Fig. 5b; $n = 25$ and n = 11, respectively).

The meiotic defects observed in each single mutant *scep1-1*, *scep2-1* and *zyp1-1* are indistinguishable (see above). We then analysed the double mutants *scep1-1 zyp1-1*, *scep2-1 zyp1-1* and *scep1-1 scep2-1* and found that they had the same phenotype as each single mutant in terms of bivalent formation defects, unequal segregation at metaphase II (Fig. 1c) and absence of synapsis (Supplementary Fig. 2). These three genes therefore act via the same pathway, and the formation of a full SC depends on each of the three proteins SCEP1, SCEP2 and ZYP1.

SCEP1 and SCEP2 form a complex

As the phenotypes of *scep1*, *scep2* and *zyp1* mutants were identical and their loading on the SC was interdependent, we wondered whether these proteins could interact together. AlphaFold2 predicted that SCEP1 and SCEP2 could form a parallel heterodimer with high interface-predicted Template Modeling (ipTM) scores and low predicted aligned error (PAE) values for the two N-terminal α-helices interacting with each other and the two C-terminal α-helices also interacting with each other (Fig. 6a). It should be noted that the disordered structure between the two α-helices of each protein is still poorly predicted when the two proteins are in a complex. Yeast two-hybrid assays confirmed that SCEP1 and SCEP2 interact with each other even on the most stringent culture media (Fig. 6b and Supplementary Table 2). Using SCEP1 and SCEP2 truncations in the yeast two-hybrid analyses, we confirmed the predicted interaction between the SCEP1 and SCEP2 C-terminal helices. However, the N-terminal helix of SCEP1 interacted only weakly with the N-terminal α-helix of SCEP2. AlphaFold2 also predicted with good

https://doi.org/10.1038/s41477-023-01558-y

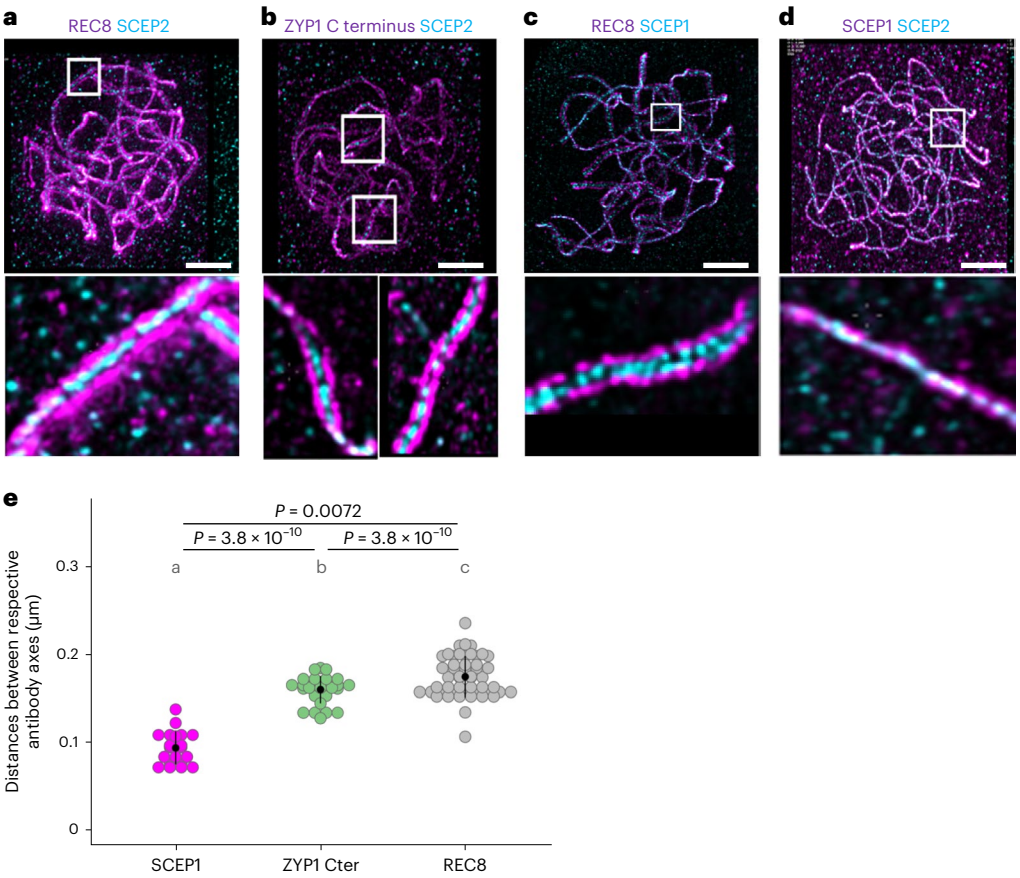

Fig. 4 | SCEP1 and SCEP2 colocalize at the centre of the SC. a, Immunolocalization of REC8 (magenta) and SCEP2 (blue) in WT male meiocytes analysed with STED microscopy. Scale bar, 2 µm. **b**, Immunolocalization of ZYP1 C terminus (magenta) and SCEP2 (blue) in WT male meiocytes analysed with STED microscopy. Scale bar, 2 µm. **c**, Immunolocalization of REC8 (magenta) and SCEP1 (blue) in WT male meiocytes analysed with STED microscopy. Scale bar, 2 µm. **d**, Immunolocalization of SCEP1 (magenta) and SCEP2 (blue) in WT male meiocytes analysed with STED microscopy. Scale bar, 2 µm. **e**, Comparison of lateral distances between observed SCEP1 lines (when applicable), ZYP1 C terminus lines (PAK133 antibody) and REC8 lines in WT plants. The black dots indicate the means, and the vertical black lines indicate the standard deviations. Different letters indicate significant differences (determined by Tukey's honestly significant difference test).

confidence the formation of parallel SCEP1 and SCEP2 homodimers (Fig. 6a), and strong interactions were detected by yeast two-hybrid assays with full-length and truncated proteins (Fig. 6b and Supplementary Table 2). We also tested whether SCEP1 and SCEP2 interacted with ZYP1. None of the SCEP1 or SCEP2 constructs, either full length or truncated, were able to interact with ZYP1 full length, N terminus or C terminus (Fig. 6b). AlphaFold2 did not predict an interface between SCEP1, SCEP2 and ZYP1 either. In yeast and mice, Ecm11 and TEX12 interact with the C-terminal parts of Zip4 and TEX11 (the mouse orthologue of the budding yeast Zip4), respectively[26]. We did not detect any interaction between the ZIP4 C terminus and SCEP1 or SCEP2 (Fig. 6b), through both yeast-two hybrid assays and AlphaFold2 predictions.

SCEP1 and SCEP2 limit class I COs and impose interference and heterochiasmy

We immunolocalized the MLH1 protein that specifically marks a subset of COs called class I COs in *scep1-1*, *scep2-1* and *scep1-1 scep2-1* male meiocytes. We observed a 50% increase in MLH1 foci in the two single mutants *scep1-1* and *scep2-1* and in the double mutant *scep1-1 scep2-1* (Fig. 7a), similar to the CO increase reported for the *zyp1* mutants[4]. To verify whether this increase in MLH1 foci reflected an increase in COs, we generated genetic maps for male and female meiosis. We crossed heterozygous *scep1-1* in the Columbia (Col-0) background with heterozygous *scep1*-7 in the Landsberg (Ler) background to produce Col-0 × Ler F_1 hybrids with two mutant *scep1* alleles. In terms of bivalent formation, the F_1 Col-0 × Ler *scep1-1 scep1-7* was indistinguishable from a Col-0 *scep1* mutant (Fig. 1c,d). These mutant F_1s were used as male or female when backcrossing with the wild-type parent Col-0.

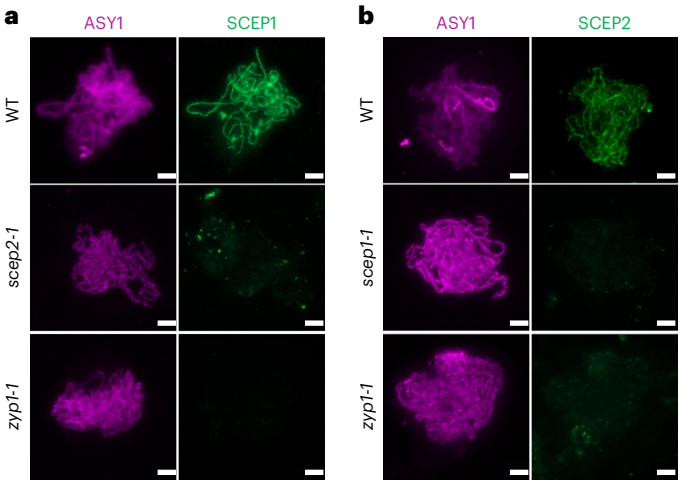

Fig. 5 | The three proteins SCEP1, SCEP2 and ZYP1 are needed to assemble the SC central region. a,**b**, Immunolocalization of ASY1 (magenta) and SCEP1 (**a**) or SCEP2 (**b**) (green) was performed in spread male meiocytes from the WT or *scep1-1*, *scep2-1* or *zyp1-1* mutants. Scale bars, 2 µm.

https://doi.org/10.1038/s41477-023-01558-y

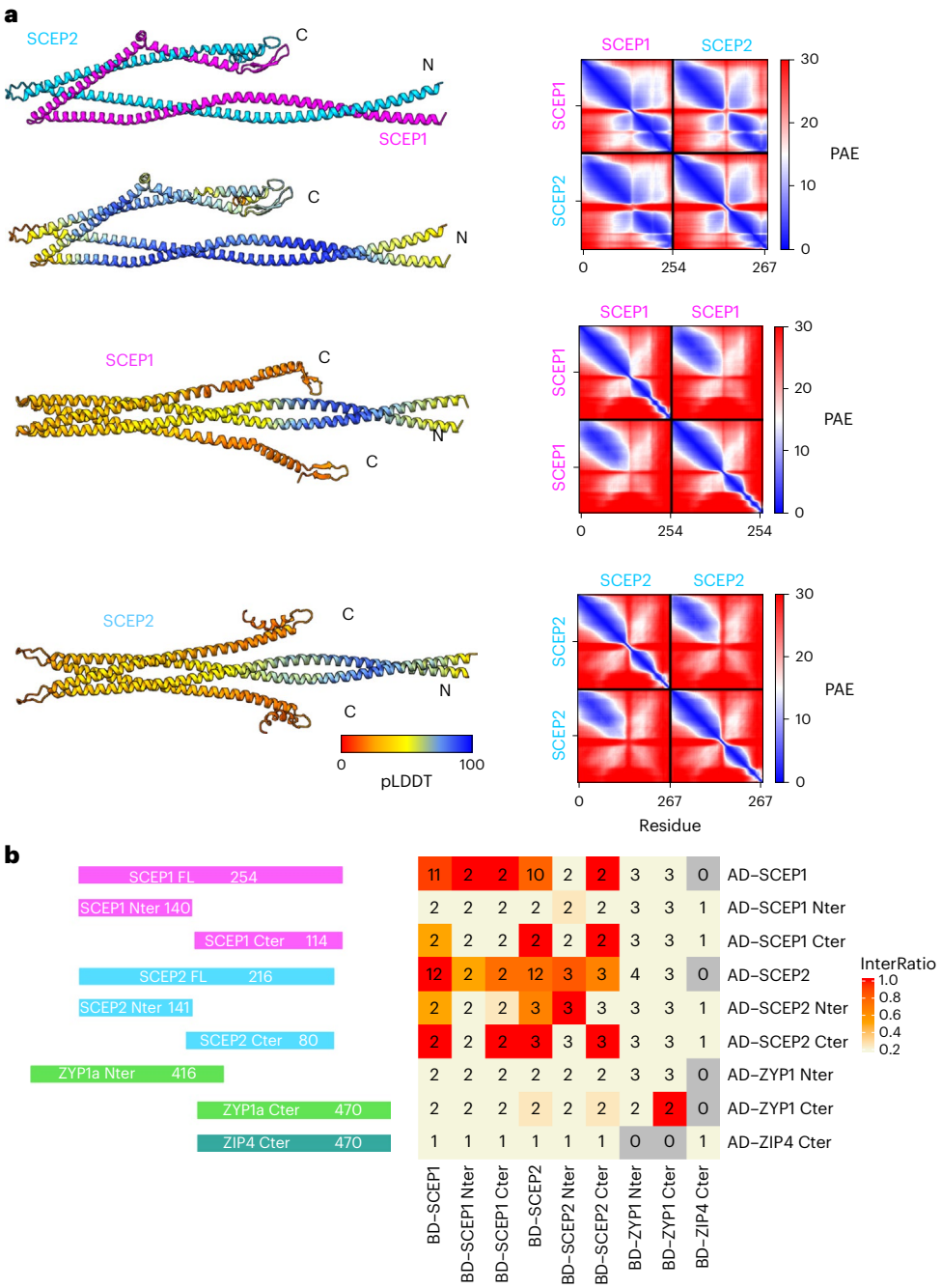

Fig. 6 | SCEP1 and SCEP2 form a complex. a, 3D model of SCEP1–SCEP2 built using the AlphaFold2 structure prediction program. Top, SCEP1 and SCEP2 heterodimers in pink and blue, respectively. Directly below, SCEP1 and SCEP2 heterodimers coloured by per-residue pLDDT. The two bottom complexes show predicted SCEP1 and SCEP2 homodimers coloured by per-residue pLDDT. High and low pLDDT values indicate strong and low confidence in the predicted structure, respectively. PAE values are shown on the right. Low PAE values indicate strong confidence in the distances between two amino acids, and high values indicate low confidence. **b**, Constructs of SCEP1, SCEP2, ZYP1A and ZIP4 used for the yeast two-hybrid assays. A heat map of the yeast two-hybrid interactions is shown on the right. The InterRatio is detailed in Methods. Red indicates that the interaction was seen on the most stringent media; light yellow indicates that no interaction was observed. The number in each tile refers to the number of repetitions of the assay. FL, full length; AD, fusion of protein sequence to yeast two-hybrid activating domain; BD, fusion of protein sequence to yeast two-hybrid DNA-binding domain.

The progeny were sequenced to obtain the number of COs and their localization. In progeny derived from *scep1-1 scep1-7* male meiosis, the average number of COs was 7.53 ± 2.3 (mean ± s.d.) per gamete ($n = 143$), confirming a large increase (+40%, Mann–Whitney test, two sides, $P < 2.2 \times 10^{-16}$) compared with the wild type (5.4 ± 1.9)[35] (Fig. 7b). This CO increase seen in *scep1-1 scep1-7* is similar to the increase in MLH1 foci observed in male meiocytes (Fig. 7a). An even higher increase was found in female meiosis with 6.6 ± 2.7 ($n = 142$) COs in *scep1-1 scep1-7*, which was far above the wild-type level (2.79 ± 1.3, $P < 2.2 \times 10^{-16}$) (Fig. 7b). In the wild type, the CO count was higher in male meiosis than in female meiosis (+90%, $P < 2.2 \times 10^{-16}$), a phenomenon called heterochiasmy. In *scep1-1 scep1-7*, the heterochiasmy was largely reduced but still significant (+14%, $P = 8.4 \times 10^{-5}$).

In *scep1*, an increase in CO frequencies was observed along chromosome arms, and particularly towards the chromosome ends (Fig. 7e). By contrast, in the pericentromeric regions, fewer COs were observed

in *scep1* than in the wild type. Both effects are clearer in female meiocytes than male meiocytes as the global CO increase is larger in female meiosis than in male meiosis (+136% versus +40% (Fig. 7b)). Thus, SCEP1 influences the CO landscape along the chromosomes in both male and female meiosis.

Interference is defined by the observation that COs do not occur close to each other on the same chromosome and are more evenly and distantly spaced than expected if distributed independently[36,37]. The observed distributions of the distances between two COs were very different in the *scep1* mutant compared with the ones observed in wild-type meiosis for both sexes. In wild-type meiosis, due to interference, COs are more widely spaced (Fig. 7c) than the expected distribution without interference (the grey distribution in Fig. 7c). By contrast, in *scep1*, in both male and female meiosis, double COs tended to occur at shorter distances and were not significantly different from the expected distribution in the absence of interference. This absence of interference in the *scep1* mutant was confirmed by plotting the coefficient of coincidence (CoC) along the chromosomes. The CoC represents the frequency of COs occurring in two different intervals of the same chromosome in a single meiosis divided by the product of the frequencies of COs in each interval (which is the expected frequency of double COs if they were independent). When the CoC equals 1, it means that a CO formed in one interval does not interfere with the occurrence of a CO in the second interval. By contrast, the closer to 0 the CoC is, the more the concomitant occurrence of two COs in two intervals is rare. In the wild type, the CoC was close to 0 when the distance between the pairs of considered intervals was shorter than 5 megabases (Mb) in male meiosis and 8 Mb in female meiosis, reflecting that interference prevents the formation of close double-CO (Fig. 7d)[4]. The CoC reached 1 at ~10 Mb in male and ~15 Mb in female wild-type meiosis, showing that interference faded at these distances. In the *scep1-1 scep1-7* mutant, the CoC curve was close to 1 regardless of the distance between intervals, in both male and female meiosis (Fig. 7d), suggesting that there is no interference in the absence of SCEP1.

The results obtained for *scep1* were compared to those obtained in the *zyp1* mutant[4]. The number of COs was not significantly different between *scep1* and *zyp1*, for both female and male meiosis ($P = 0.08$ and 0.05, respectively) (Fig. 7b); interference was abolished in both contexts (Fig. 7c,d)[4]; and the CO distributions were comparable (Fig. 7e and Extended Data Fig. 3). However, heterochiasmy was strongly reduced but not abolished in *scep1*, with male gametes having only 14% more COs than female gametes ($P < 0.001$), compared with +94% in the wild type ($P < 0.0001$) and the absence of heterochiamsy in *zyp1* ($P = 0.32$).

SCEP1 and SCEP2 homologues are found in angiosperms

Through a PSI-BLAST approach, the presence of SCEP1 and SCEP2 homologues was inferred on the basis of sequence identity in a representative set of plant species. Homologues for both SCEP1 and SCEP2 were found in all major angiosperm clades, including the basal angiosperm *Amborella trichopoda* (Fig. 8). Outside angiosperms, homologues were also found in *Selaginella moellendorffii*. Reciprocal PSI-BLAST best-hit searches starting from the homologues found in *Selaginella* and in the chosen angiosperms *Amborella*, *Jatropha curcas*, *Solanum lycopersicum* and *Gossypium raimondii* were performed and confirmed that these are indeed SCEP1 and SCEP2 homologues, since the only homologues found in *Arabidopsis* are SCEP1 and SCEP2, respectively. Moreover, the SCEP1 and SCEP2 homologues found in the above species were predicted to interact with significant confidence levels using AlphaFold2 (ipTM scores of 0.7, 0.6, 0.5, 0.6 and 0.5, respectively; Extended Data Fig. 4). Beyond flowering plants (angiosperms) and lycophytes (*S. moellendorffii*), the sequence search was not sensitive enough to find SCEP1 and SCEP2 homologues. As previously reported[38], ZYP1 homologues were found in all angiosperms as well as in the gymnosperm *Taxus chinensis* and the bryophyte *Marchantia polymorpha*.

Discussion

In contrast to animals and fungi, no protein specific to the CE of the SC was known in plants. Here we describe the identification of two new meiotic proteins, SCEP1 and SCEP2. These proteins are small coiled-coil proteins. They both localize in the middle of the central region of the SC, together with the N-terminal part of ZYP1. The localizations of the three proteins, SCEP1, SCEP2 and ZYP1, depend on each other. Moreover, the meiotic defects observed in the *scep1* and *scep2* mutants phenocopy the ones reported in the *zyp1* mutant[4,5]: pairing of homologous chromosomes but no synapsis, CO increase but loss of interference, and reduction of heterochiasmy. In addition, COs are redistributed in a similar way to *zyp1* with an increase of distal COs and a reduction of pericentromeric COs. All these data led us to conclude that SCEP1 and SCEP2 are CE proteins that have now been identified and characterized in plants.

Described CE proteins are known to associate and form subcomplexes: Ecm11 with Gmc2 (ref. 20), Cona with COROLLA[21,29], SYP-3 with SYP-4 (ref. 28), SYCE1 with SIX6OS1 (ref. 16) and SYCE2 with TEX12 (ref. 15). We demonstrated that SCEP1 and SCEP2 interact with each other in yeast two-hybrid assays, and AlphaFold2 predicts that they could form a heterodimer. Previously described CE proteins often form multimers of higher orders than two. For example, SYCE2–TEX12 forms tetramers and can further assemble into fibres that could form the midline structure of the SC[27]. SYCE3 self-assembles in tetramers that can form higher-order structures[39]. When AlphaFold2 was run with different stoichiometries of SCEP1 and SCEP2, heteromeric assemblies were systematically preferred over homomeric ones, and none of the AlphaFold2 predictions suggested a model including homodimers and heterodimers. The hetero tetramer model of SCEP1 and SCEP2 in a 2:2 stoichiometry resulted in a complex interlaced assembly (Supplementary Fig. 4), suggesting how multimers of a higher order could be formed. We also observed that even if the two proteins are very often found to colocalize, they may show some differences, with SCEP1 that seems to encompass SCEP2 at some positions. This result suggests that SCEP1 and SCEP2 do not solely form a parallel dimer or a tetramer, but possibly a more complex structure with SCEP2 homodimers or multimers at the centre connected directly or indirectly to

Fig. 7 | MLH1 foci and COs are increased in CE mutants. a, MLH1–HEI10 foci were quantified following a triple immunolocalization ASY1–MLH1–HEI10 performed on WT ($n = 184$), *scep1-1* ($n = 93$), *scep2-1* ($n = 114$) and *scep1-1 scep2-1* ($n = 72$) male meiocytes and imaged with an epifluorescence microscope. Each dot indicates an individual cell, and the red bar indicates the mean. Tukey's multiple comparison test was used to determine significance. Only P values <0.01 are shown (Supplementary Table 10). **b**, The number of COs detected following whole-genome sequencing of female and male backcrosses of Col/Ler F_1 hybrids. Each dot indicates an individual BC1 plant, the mean value of each population is indicated at the top and the population size is shown in parentheses. The two-sided Mann–Whitney test was used to evaluate the differences in CO numbers. **c**, Distributions of inter-CO distances for chromosomes having exactly two COs. The grey bars represent the expected distribution of COs in the absence of interference, as calculated by permuting the CO positions between gametes. The number of analysed events and the P value from the Mann–Whitney test comparing observed and expected distributions are indicated in parentheses. **d**, Chromosomes were divided into 15 intervals, and the mean CoC was calculated for pairs of intervals separated by a certain distance (Mb). **e**, The distribution of COs along chromosome 1 in female and male WT, *zyp1* and *scep1-1*. The other chromosomes are presented in Extended Data Fig. 3. The centromere and pericentromeric regions are indicated by grey and blue shading, respectively. The analysis was done with 1-Mb windows and 50-kb sliding steps. For pericentromeric regions and each non-overlapping 1-Mb window along the chromosome arms, Pearson's chi-squared test was used to examine the difference between the WT and *scep1-1*. Windows with P value (corrected with the false discovery rate method) <0.05 are marked by asterisks.

https://doi.org/10.1038/s41477-023-01558-y

SCEP1 homodimers or multimers nearby. We could hypothesize that additional proteins or protein modifications could be involved to strengthen these interactions. Alternatively, even if the polyclonal antibodies were raised against full-length proteins, they may preferentially label part of the proteins, leading to a misinterpretation of their relative localization. Further analyses including structural biochemistry and super-resolution microscopy with a series of specific antibodies will be needed to infer the structure that the SCEP1–SCEP2 complex adopts.

In *scep1* or *scep2* mutants, no trace ZYP1 was detected on the SC, which strongly suggests that SCEP1 and SCEP2 are needed for the assembly of TFs. In other species, CE subcomplexes play different roles in SC assembly. In the absence of SYCE2 or TEX12 in mice, or Ecm11 or Gmc2 in budding yeast, chromosomes align, and the TF protein SYCP1 or Zip1 localizes at synapsis initiation sites, but synapsis does not extend[20,40,41]. In the absence of SYCE1 or SIX6OS1 or SYCE3 in mice, there are no initiation synapsis sites, and SYCP1 loads on AE in a discontinuous

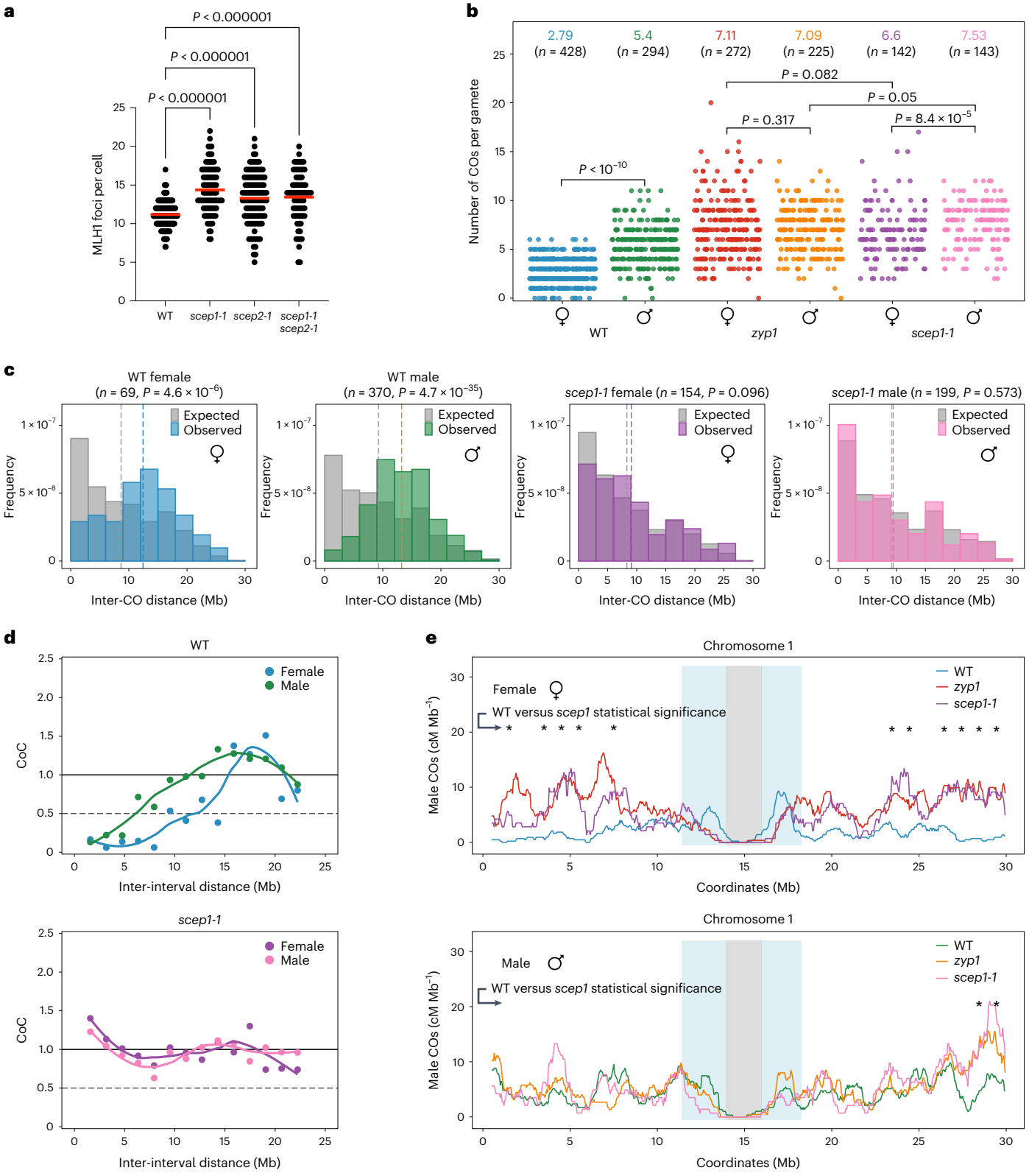

https://doi.org/10.1038/s41477-023-01558-y

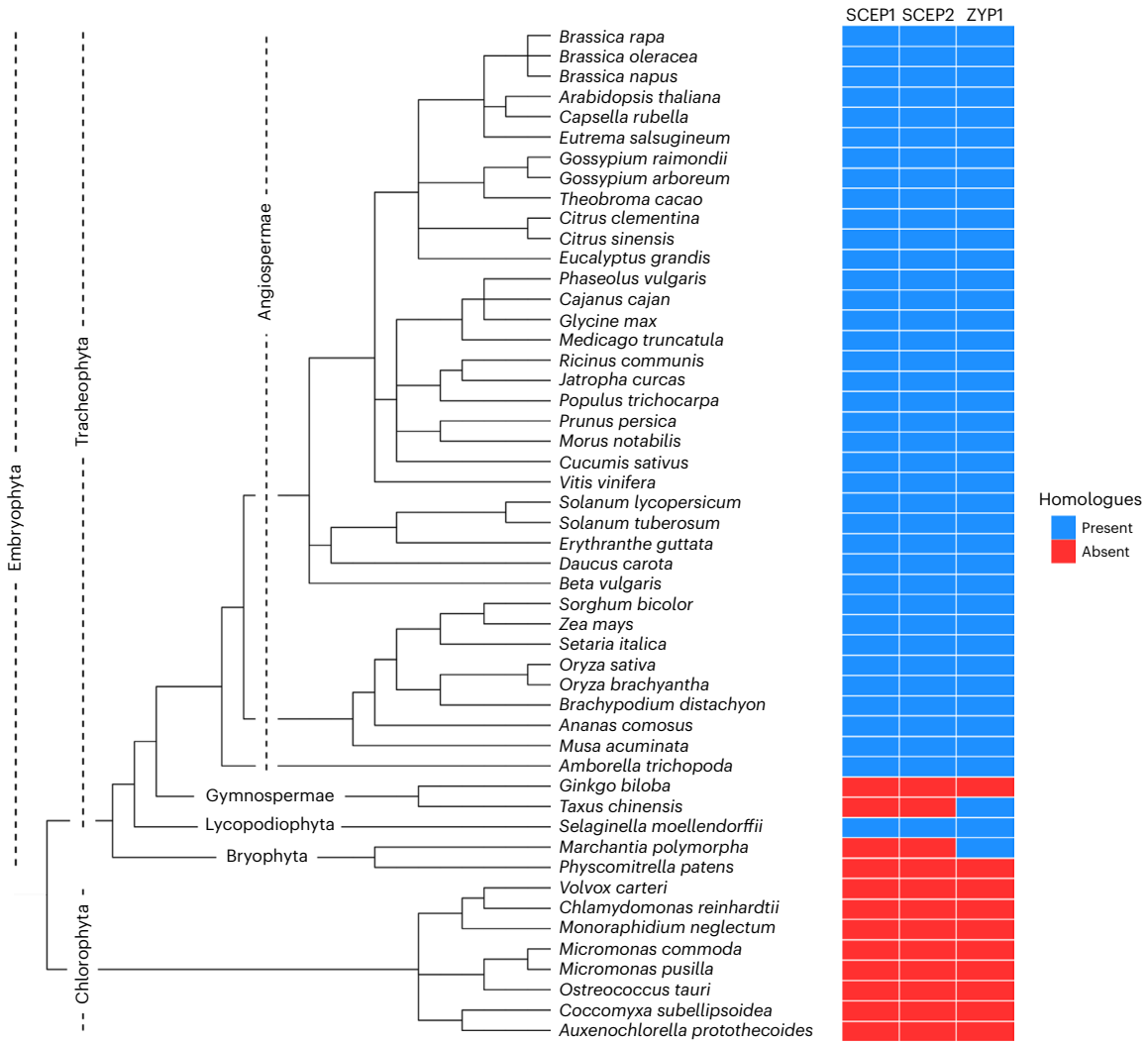

Fig. 8 | SCEP1, SCEP2 and ZYP1 homologues can be found in all major angiosperm species. The heat map indicates the presence or absence of SCEP1, SCEP2 or ZYP1 homologues determined through a PSI-BLAST approach. An additional classification of 'unsure' homologues was added (Methods). Viridiplantae phylogenetic tree adapted from ref. 67 under a Creative Commons license CC BY 4.0.

pattern but is unable to form head-to-head polymers[14,16,42]. Therefore, as no SC initiation is observed in *scep1* and *scep2* mutants, the SCEP1–SCEP2 dimer seems to be functionally closer to the mouse SYCE1–SIX6OS1 than to SYCE2–TEX12/Ecm11–Gmc2. Moreover, Ecm11 and TEX12 interact with Zip4 and TEX11 (the mouse orthologue of the budding yeast Zip4)[26], and we did not detect any interaction between ZIP4 and SCEP1 or SCEP2, even though the Zip4 protein motif involved in this interaction is conserved in *A. thaliana*. Other CE proteins, not yet identified, could play the role of SYCE2–TEX12/Ecm11–Gmc2.

The similarity in ZYP1, SCEP1 and SCEP2 localizations at the centre of the SC; the interdependence of each of the three proteins on the two others for their presence on the SC; and the perfect similarity between *zyp1*, *scep1* and *scep2* mutant phenotypes suggest that they could form a complex. However, no interactions were detected between the SCEP1–SCEP2 dimer and ZYP1, both through yeast two-hybrid assays and AlphaFold2. A possible reason is the poor ZYP1 structure prediction by AlphaFold2. Instead of the extended linear coiled-coil protein clearly demonstrated in biochemical and cytological studies with the N-terminal part and C-terminal part on opposite sides, AlphaFold2 computes a folding in the middle of the protein between two coiled-coil domains leading to a proximity of the N- and C-terminal parts. We were also unable to detect any interaction by yeast two-hybrid assays both with full-length proteins and with truncated proteins. Nevertheless, in other species, not all CE subcomplexes have been shown to interact with their corresponding TF proteins. In mice, SYCE3 interacts with SYCP1 by yeast two-hybrid but not SYCE1, SYCE2, TEX12 or SIXOS1 (ref. 25). In yeast, no interaction was found between either Ecm11 or Gmc2 and Zip1 by co-immunoprecipitation or yeast two-hybrid assays[26]. In *C. elegans*, SYP-2 and SYP-3 interact with SYP-1 by yeast two-hybrid but not SYP-4 (ref. 18), whereas co-immunoprecipitation analyses have shown that two complexes are formed, one containing SYP-5 and the other SYP-6, with SYP-5 and SYP-6 interacting with SYP1 and SYP3 but not with SYP-4 and SYP-2 (ref. 10). Recently, the SC structure has been revisited, and what was thought to be a fixed, simple ladder-like structure with a few structural proteins is now thought to be more dynamic and includes a series of regulatory protein complexes[10,43]. In both yeast and worms, the central region of the SC, but not the axes, appears to have fluid-like properties[43], where the weakly bound proteins can move within the structure. We can therefore hypothesize that the SCEP1–SCEP2 complex interacts only transiently with ZYP1 and that further analyses would be needed to reveal these interactions. Alternatively, protein modifications may be needed to mediate interactions within the SC. In *S. cerevisiae*, Zip1 and the two CE proteins Ecm11 and Gmc2 have been found to be highly sumoylated, and Ecm11 sumo modification is needed for SC polymerization[20,44,45]. In mice, SUMO modifications decorate axes and SC central regions

along chromosomes, and inhibiting SUMO conjugation causes synapsis defects[46]. Alternatively, one or more yet-unidentified *Arabidopsis* proteins could mediate the interactions between the TFs and the CE proteins SCEP1 and SCEP2.

In budding yeast, mice, *C. elegans*, *Drosophila* and *Sordaria macrospora*[7,11,17,47–49], the TF protein is required for class I CO formation. By contrast, in the absence of TFs in rice and *Arabidopsis*, a clear increase in the number of ZMM-promoted COs is observed[4,5,50], but they completely lose interference, and the obligatory CO is lost. COs are thus randomly distributed among bivalents, explaining why even with a 50% increase in COs, COs form in excess in some bivalents whereas other bivalents do not receive a single CO, producing univalents that segregate randomly at the first meiotic division. In the *scep1* mutant, the number of COs showed a comparable increase to that of *zyp1* (refs. 4,5), and they did not exhibit interference. This further supports the conclusion that the tripartite SC itself is essential to imposing CO interference in *Arabidopsis*. Our data are compatible with the 'coarsening' model proposed recently in *Arabidopsis* and *C. elegans*, where the TFs would provide an interface acting as a 'railway' along which the ZMM pro-CO factors (such as HEI10) diffuse, and bind to recombination intermediate sites[51–55]. Different rates of association and dissociation from recombination sites creates a local accumulation of HEI10 at a few sites that will become COs at the expense of neighbouring sites, leading to CO interference. In *scep1*, the TFs are not formed, and as proposed for *zyp1* mutants, HEI10 is not constrained on the SC; HEI10 binds to recombination intermediates and coarsens at the expense of the nucleoplasm pool, allowing COs to be formed close by[51–55]. In this coarsening model, heterochiasmy relies on the size of the SC, which is smaller in *Arabidopsis* female meiosis and thus accumulates less HEI10 foci than in male meiosis, which has a longer SC. In the absence of the ZYP1 'railway', the SC is no longer the metric for the HEI10 dynamic, and heterochiasmy is not maintained in *scep1*$^{-/-}$, just as in *zyp1-1* (ref. 4).

Orthologues of SCEP1 and SCEP2 have been found in all the species or at least in one representative species of the various families of vascular plants, except in gymnosperms. Outside Tracheophytes, no convincing homologues were detected. However, a recent study[38] detected ZYP1 in all the lineages of Viridiplantae, including gymnosperms. Our data suggest that the three proteins SCEP1, SCEP2 and ZYP1 form a functional triad and could therefore be expected to be found together. As potential (although unsure) ZYP1 homologues could be identified in the species without SCEP1 or SCEP2 homologues, it can be hypothesized that SCEP1 and SCEP2 homologues do exist but exhibit high sequence divergence compared with the *Arabidopsis* SCEP1 and SCEP2 sequences. In this scenario, all known SC proteins may derive from common ancestors, but sequence divergence makes them unrecognizable with the current tools used for sequence similarity analyses. Alternatively, TF and/or CE proteins could have emerged independently during evolution and been selected on their 3D structure to assemble and synapse chromosomes. Further homology searches based on the structure of these proteins may shed a clearer light on the composition of the central region in these species.

Methods

Plant materials and growth conditions

A. thaliana plants were grown in greenhouses with 70% humidity and under a 16 h/8 h day/night photoperiod with temperatures of 19 °C during the day and 16 °C at night. Wild-type Col-0 and Ler-1 are 186AV1B4 and 213AV1B1 from the Versailles *A. thaliana* stock centre (http://publiclines.versailles.inra.fr/). The *zyp1-1* mutant was described previously[4]. Heterozygous *scep1-1*$^{+/-}$ plants were crossed with heterozygous *scep1-7*$^{+/-}$ plants to produce *scep1-1 scep1-7* heteroallelic homozygous mutants. These plants were backcrossed as male or female with wild-type Col-0 to generate the sequencing populations. The backcross populations were treated as described previously[51]. The four T-DNA insertion lines in AT3G28370 were provided by the Nottingham Arabidopsis Stock Centre (http://nasc.nott.ac.uk/). Neither the line before the ATG (PST16975) nor the two lines with an insertion in the last intron (N525173 and N508352) that are predicted to only remove the last five amino acids of the long isoform (Extended Data Fig. 1e,f) showed any univalent on at least 50 different metaphase I meiotic cells. The line N663933 (*scep2-1*) was further characterized. To generate the double homozygous *scep1-1*$^{-/-}$ *scep2-1*$^{-/-}$, heterozygous *scep1-1*$^{+/-}$ and *scep2-1*$^{+/-}$ plants were crossed. The obtained double heterozygous *scep1-1*$^{+/-}$ *scep2-1*$^{+/-}$ were selfed to produce double homozygous *scep1-1*$^{-/-}$ *scep2-1*$^{-/-}$, the single mutants *scep1-1*$^{-/-}$ and *scep2-1*$^{-/-}$, and wild-type plants. These sister plants were used to perform MLH1 foci counting. Double homozygous plants *scep1-1*$^{-/-}$ *zyp1-1*$^{-/-}$ and *scep2-1*$^{-/-}$ *zyp1-1*$^{-/-}$ were obtained after crossing heterozygous plants for each mutation. After selfing, double mutants were selected. The genotyping conditions used in that study are listed in Supplementary Table 3.

Expression data

Transcriptomic data were downloaded from https://datacommons.cyverse.org/browse/iplant/home/araport/rnaseq_bam/Klepikova and analysed using an in-house R (4.2.2) script. The data were filtered to retain only the expression levels in flowers (stages 1 through 19, corresponding to buds from under 0.3 mm to more than 3 mm as defined in ref. 30). Differential gene expression analysis was performed with the edgeR (3.42.4) package, and the normalization was done by the trimmed mean of M-values method. As known meiotic genes displayed peak expression at stage 15 (buds between 0.3 and 0.5 mm), genes that had a mean value at stage 15 at least 1.8 times higher than the mean values at stages 1 (buds >3 mm), 2 (buds between 2.6 and 2.9 mm) and 3 (buds between 2.1 and 2.5 mm) and where the mean value at stage 15 was the highest among all other flower stages were selected, corresponding to almost 250 genes. To narrow down the number of genes obtained and make the screen doable, genes that had an expression level above that of *DMC1* and below that of *SPO11-2* (the most and least expressed meiotic genes) were filtered out, and the 80 genes exhibiting a mean root expression level lower by at least 30% than that observed during flower stage 15 were retained.

PCR with reverse transcription experiments

Total RNA extracted from flower buds was prepared and purified using the RNeasy Plant Mini Kit (Qiagen) according to the manufacturer's instructions. Complementary DNAs were synthesized out of 1 µg of total RNA using an oligo-dT18 primer and the RevertAid RT Reverse Transcription Kit (ThermoFisher Scientific) according to the manufacturer's instructions. Complementary DNAs were used to amplify the 3′ extremity of SCEP1 (RT_SCEP1_fwd/RT_SCEP1_rev) or SCEP2 (RT_SCEP2_fwd/RT_SCEP2_rev1 or RT_SCEP2_fwd/RT_SCEP2_rev2). The PCR fragments were Sanger sequenced (Genoscreen).

Generation of the CRISPR–Cas9 *scep1* mutants

Three gRNAs targeting the At*SCEP1* gene (AT1G10710) were designed with CRISPOR (http://tefor.net/crispor/crispor.cgi)[56]. Expression cassettes sgRNA_SCEP1#1, sgRNA_SCEP1#2 and sgRNA_SCEP1#3 including Gateway recombination sites were synthesized by Twist Biosciences and inserted in the pDE–Cas9–DSred vector[57,58] by LR reaction using the Gateway technology (Invitrogen). The resulting construct was transformed into *A. thaliana* ecotype Col-0 plants or Ler plants using the floral dip method[59]. Plant transformants (T_1) were selected by seed fluorescence, and 20 transformants were transferred to the greenhouse. The progeny without fluorescence were selected and screened for mutations by PCR amplification (SCEP1_RP1/ SCEP1_LP1 or SCEP1_RP2/ SCEP1_LP2) and Sanger sequencing at the targeted locus. Seven independent lines carrying homozygous frameshift mutations were used for further characterization.

Yeast two-hybrid assays

The DNA sequences corresponding to SCEP1, the first 217 amino acids of SCEP2 and the last 469 amino acids of ZIP4 were chemically synthesized (Twist Biosciences). attB1 and attB2 recombinant tails were added to these fragments to transfer them into pDONOR207 using the Gateway technology (Invitrogen). Truncations of SCEP1 or SCEP2 were generated by PCR using specific primers flanking the attB1 and attB2 recombination sites and cloned into pDONOR207. After sequencing, the entry vectors were used to generate the appropriate pGAD and pGBK yeast two-hybrid expression vectors. These were transformed into AH109 and Y187 strains, respectively, by heat shock, and grown on selective media (without leucine for transformed AH109 and without tryptophan for transformed Y187). Conjugations were carried out in liquid non-selective media overnight and then grown on solid media lacking both leucine and tryptophan (SD-LW). Each interaction was tested by taking eight separate yeast colonies grown on SD-LW and resuspending them in eight separate 100 µl water wells. 10 µl of these were then successively deposited on solid SD-LW, SD-LWH (SD-LW without histidine) and SD-LWHA (SD-LWH without adenine). Two proteins were deemed to interact when the eight separate spots grew on SD-LWH and/or SD-LWHA and no self-activation could be observed.

The DNA sequences corresponding to the 416 first amino acids of ZYP1a (ZYP1aNter) or the 469 last amino acids of ZYP1a (ZYP1aCter) were chemically synthesized (Twist Biosciences). attL1 and attL2 recombinant tails were added to these fragments to transfer them directly into the yeast two-hybrid expression vectors using the Gateway technology (Invitrogen). Details on the constructs are provided in Supplementary Table 4.

To simplify the visualization of the interaction results, a scoring of each protein pair is used, called the InterRatio. This ratio reflects the number of times an interaction is observed with respect to the number of times it was tested. Interactions observed due to self-activation are not considered, and only interactions that also grew on the LW medium are considered. To fit the data collected, a weighting is done to reflect whether the interaction was observed on LWHA or only on LWH, the latter reflecting a weaker interaction.

$$\text{InterRatio} = \frac{n\,(\text{LWHA}) + \frac{1}{2}n(\text{LWH})}{n(\text{Tests})}$$

Here, n(LWHA) is the number of times the interaction is observed on the LWHA medium, n(LWH) is the number of times the interaction is observed only on the LWH medium (meaning not on the LWHA medium) and n(Tests) is the number of times the interaction was tested (always greater than 0). For example, for an interaction between two proteins A and B that show no self-activation and for which two interaction tests were performed, one showing an interaction on LWH and LWHA while the second test showed an interaction only on the LWH medium, the InterRatio takes a value of $\frac{1+\frac{1}{2}\times 1}{2} = 0.75$. This is only computed because the yeasts also grew on the LW medium. The InterRatio is computed in an R (4.2.2) script that takes Supplementary Table 2 as its input and produces the corresponding InterRatio heat map.

AlphaFold2 predictions

AlphaFold2 predictions of both monomers and multimers were computed through the ColabFold notebook (ColabFold v.1.3 and AlphaFold2 v.2.2) using a ColabPro+ plan (https://colab.research.google.com/github/sokrypton/ColabFold/blob/main/AlphaFold2.ipynb). The plDDT, PAE and ipTM scores and graphs were provided directly by this notebook. The predicted structures were not relaxed using amber, and no template information was used. mmseqs_uniref_env was used for the unpaired MSA, and sequences from the same species were paired. For the advanced settings, the automatic modes were applied, only one seed was used and dropouts were not enabled. Images were produced using UCSF ChimeraX[60].

Production of anti-SCEP1, SCEP2 or ZYP1-Cter antibodies

The cDNA of SCEP1 or SCEP2 inserted in pDONOR207 was transferred into the expression plasmid pDEST17 (Novagen) using the Gateway technology (Invitrogen). The resulting plasmids were used to transform the *E. coli* expression strain BL21 ER2566 (New England Biolabs). Protein expression was induced at 37 °C for 3 h, and recombinant protein was resolubilized as described in ref. 61. Rabbit anti-SCEP1 or rat anti-SCEP2 antibodies were obtained (Eurogentec) and used at a dilution of 1:200 for immunofluorescence. The ZYP1 polyclonal Cter antibody (lab name, PAK133) was produced against the peptide CEGSLNPYADDPYAFD, which is located at the very C-terminal end of the ZYP1 proteins. It was raised in rabbit and affinity purified using the 28-day programme of Eurogentec.

Cytology

Seeds were counted after silique clearing in 70% ethanol. Meiotic chromosome spreads were DAPI stained as described previously[62]. For each genotype, DAPI staining was performed on spreads obtained from pooled anthers from 10 to 20 flowers on one plant for *scep1-1*, *scep1-2*, *scep1-3*, *scep1-4* and *scep1-5*; two plants for *scep1-6*, *zyp1-1*, *scep1-1 scep2-1*, *scep1-1 zyp1-1* and *scep2-1 zyp1-1*; and four plants for the wild type and *scep1-7*. Immunolocalization was performed either on 2D lipsol male meiotic spreads as described in ref. 63 or on 3D preserved cells as described in refs. 31,51. For immunostaining, eight primary antibodies were used for both epifluorescence and super-resolution microscopy: anti-REC8 raised in rat or in rabbit[64] (dilution 1:250), anti-MLH1 in rabbit[61] (dilution 1:1,000), anti-HEI10 in chicken (dilution 1:10,000)[51], anti-ASY1 in guinea pig[31](dilution 1:250), anti-ZYP1 in rat[3] (dilution 1:250), anti-ZYP1-Cter PAK133 in rabbit (dilution 1:200, this study), anti-SCEP1 in rabbit (dilution 1:200, this study) and anti-SCEP2 in rat (dilution 1:200, this study). Secondary antibodies were conjugated with Alexa 488, Alexa 568 or Alexa 647 for epifluorescence and Abberior STAR Red (1/500) or STAR Orange (1/500) for STED microscopy (Supplementary Table 12).

Images were taken using a Zeiss Axio Observer microscope. MLH1 immunofluorescence studies were carried out on 3D preserved meiocytes as described previously[31]. Super-resolution images were acquired using the Abberior STEDYCON system. Super-resolution images were acquired with the Abberior instrument facility line (https://abberior-instruments.com/) with 561 and 640 nm excitation lasers (for STAR Orange and STAR Red, respectively) and a 775 nm STED depletion laser. Confocal images were taken with the same instrument with a 485 nm excitation laser (for STAR GREEN/Alexa 488).

Image processing and analysis

Deconvolution of the images was performed by Huygens Essential (v.21.10, Scientific Volume Imaging, https://svi.nl/) using the classic maximum likelihood estimation algorithm with lateral drift stabilization, a signal-to-noise ratio of 7 for STED images and 20 for confocal images, 40 iterations, and a quality threshold of 0.5. Maximum intensity projections and contrast adjustments were also done with Huygens Essential 22.04.0p0 64b. Deconvoluted pictures were imported into Imaris x64 9.6.0 (https://imaris.oxinst.com/, Oxford Instruments) for subsequent analysis. MLH1 foci were counted in diplotene and diakinesis cells. The vast majority of MLH foci colocalize with a HEI10 focus. Only double MLH1/HEI10 foci present on chromosomes were taken into account.

For measuring distances between REC8-labelled axial bridges, ten independent cells (four for each mutant and two for the wild type) and 25 counts were recorded. Lines (width = 3) were drawn on random seemingly flat regions using ImageJ 2.9.0. For each line, the greyscale intensity profile was exported from ImageJ 2.9.0. and analysed in R.

The lines were then individually fitted using a local polynomial regression (loess function, stats package) with a span of 0.5. The *x* values of the two local maxima given by the fitted values were recorded for each line, and the distance between the two axes was deduced. Since homologous chromosomes in mutants were never fully aligned, the lines were drawn on regions where chromosomes were the closest 'by eye' to each other. The overall distance between homologous chromosomes in mutants is therefore underestimated.

The same strategy was used to calculate the distance between occasional SCEP1 double lines and between the ZYP1 C-terminal section.

CO analysis

The previously described method was followed for the generation of high-confidence SNP markers between Col and Ler, mapping of sequencing reads, meiotic CO prediction, and filtering of the poorly covered and potentially contaminated samples[4,35,51,65,66]. The identified COs were then manually and randomly checked by using inGAP-family[65]. A total of 937 and 1,077 COs were identified from the 142 and 143 *scep1* female and male plants (ArrayExpress number E-MTAB-12985), respectively. The list of 1,192 and 1,587 COs of the wild-type female and male populations (428 and 294 plants, ArrayExpress number E-MTAB-11254) and the list of 1,933 and 1,596 COs of the *zyp1* female and male populations (272 and 225 plants, ArrayExpress number E-MTAB-9593, E-MTAB-11696) from the previous studies[4,35,51] were used for the analysis of CO number and distribution and CO interference, following the previous descriptions[4,51]. The list of CO positions can be found in Supplementary Table 7. The raw read data for Fig. 7 can be found in the EBI ArrayExpress database under accession number E-MTAB-12985 (https://www.ebi.ac.uk/biostudies/studies/E-MTAB-12985).

SCEP1 and SCEP2 orthologues

Arabidopsis protein sequences from SCEP1 (AT1G33500), SCEP2 (AT3G28370) and ZYP1b (AT1G22275) were taken from the TAIR website, while protein sequences from other species were taken from the National Center for Biotechnology Information (NCBI) accessions. NCBI PSI-BLASTs against Viridiplantae were used to search for SCEP1 and SCEP2 homologues, with an *E*-value threshold of 5×10^{-3} and BLOSUM62 matrix. Two iterations were performed, and proteins with an *E* value less than 10×10^{-10} and a per cent identity greater than 10% were considered potential homologues. Proteins that were smaller than 100 amino acids and larger than 500 were also filtered out. The same strategy was used for ZYP1, but a single iteration was performed, and proteins below 450 amino acids were discarded. Lowering the *E*-value threshold for homologue consideration to 5×10^{-3} did not modify the results shown in Fig. 8. A description of the homologues can be found in Supplementary Table 6. A reciprocal best-hit strategy with identical BLAST parameters was used to confirm the presence of homologues in *S. moellendorffii*, *A. trichopoda*, *J. curcas*, *S. lycopersicum* and *G. raimondii*. The PSI-BLASTs targeted at individual species from Fig. 8 for which no SCEP1, SCEP2 and/or ZYP1 homologue had initially been found were performed with identical parameters. The PSI-BLAST results were downloaded and analysed using in-house R (4.2.2) scripts to filter and rank homologues, quantify their presence or absence in the different species, fetch the protein sequences, and draw the phylogenic tree and the associated matrix. The phylogenic tree was taken from ref. 67, from which a subset of Viridiplantae was made. The two gymnosperms and *Marchantia* were added according to NCBI taxonomy and the phylogeny proposed by refs. 68,69. No phylogenic tree prediction was made in our analysis; only the presence or absence of SCEP1, SCEP2 and ZYP1 in major plant species was investigated.

Reporting summary

Further information on research design is available in the Nature Portfolio Reporting Summary linked to this article.

Data availability

The raw read data for Fig. 7 can be found in the EBI ArrayExpress database under accession number E-MTAB-12985 (https://www.ebi.ac.uk/biostudies/studies/E-MTAB-12985).

Code availability

The in-house R (4.2.2) scripts used in this work are available at https://github.com/mapeuch/SCEP1_SCEP2_paper.

References

1. Zickler, D. & Kleckner, N. Recombination, pairing, and synapsis of homologs during meiosis. *Cold Spring Harb. Perspect. Biol.* **7**, a016626 (2015).
2. Schmekel, K. et al. Organization of SCP1 protein molecules within synaptonemal complexes of the rat. *Exp. Cell. Res.* **226**, 20–30 (1996).
3. Higgins, J. D., Sanchez-Moran, E., Armstrong, S. J., Jones, G. H. & Franklin, F. C. H. The *Arabidopsis* synaptonemal complex protein ZYP1 is required for chromosome synapsis and normal fidelity of crossing over. *Genes Dev.* **19**, 2488–2500 (2005).
4. Capilla-Pérez, L. et al. The synaptonemal complex imposes crossover interference and heterochiasmy in *Arabidopsis*. *Proc. Natl Acad. Sci. USA* **118**, e2023613118 (2021).
5. France, M. G. et al. ZYP1 is required for obligate cross-over formation and cross-over interference in *Arabidopsis*. *Proc. Natl Acad. Sci. USA* **118**, e2021671118 (2021).
6. Sym, M., Engebrecht, J. A. & Roeder, G. S. ZIP1 is a synaptonemal complex protein required for meiotic chromosome synapsis. *Cell* **72**, 365–378 (1993).
7. Vries, F. A. T. D. et al. Mouse Sycp1 functions in synaptonemal complex assembly, meiotic recombination, and XY body formation. *Genes Dev.* **19**, 1376–1389 (2005).
8. MacQueen, A. J., Colaiacovo, M. P., McDonald, K. & Villeneuve, A. M. Synapsis-dependent and -independent mechanisms stabilize homolog pairing during meiotic prophase in *C. elegans*. *Genes Dev.* **16**, 2428–2442 (2002).
9. Hurlock, M. E. et al. Identification of novel synaptonemal complex components in *C. elegans*. *J. Cell Biol.* **219**, e201910043 (2020).
10. Zhang, Z. et al. Multivalent weak interactions between assembly units drive synaptonemal complex formation. *J. Cell Biol.* **219**, e201910086 (2020).
11. Page, S. L. & Hawley, R. S. c(3)G encodes a *Drosophila* synaptonemal complex protein. *Genes Dev.* **15**, 3130–3143 (2001).
12. Dong, H. & Roeder, G. S. Organization of the yeast Zip1 protein within the central region of the synaptonemal complex. *J. Cell Biol.* **148**, 417–426 (2000).
13. Costa, Y. et al. Two novel proteins recruited by synaptonemal complex protein 1 (SYCP1) are at the centre of meiosis. *J. Cell Sci.* **118**, 2755–2762 (2005).
14. Schramm, S. et al. A novel mouse synaptonemal complex protein is essential for loading of central element proteins, recombination, and fertility. *PLoS Genet.* **7**, e1002088 (2011).
15. Hamer, G. et al. Characterization of a novel meiosis-specific protein within the central element of the synaptonemal complex. *J. Cell Sci.* **119**, 4025–4032 (2006).
16. Gómez-H, L. et al. C14ORF39/SIX6OS1 is a constituent of the synaptonemal complex and is essential for mouse fertility. *Nat. Commun.* **7**, 13298 (2016).
17. Colaiacovo, M. P. et al. Synaptonemal complex assembly in *C. elegans* is dispensable for loading strand-exchange proteins but critical for proper completion of recombination. *Dev. Cell* **5**, 463–474 (2003).

18. Smolikov, S., Schild-Prufert, K. & Colaiacovo, M. P. A yeast two-hybrid screen for SYP-3 interactors identifies SYP-4, a component required for synaptonemal complex assembly and chiasma formation in *Caenorhabditis elegans* meiosis. *PLoS Genet.* **5**, e1000669 (2009).
19. Smolikov, S. et al. SYP-3 restricts synaptonemal complex assembly to bridge paired chromosome axes during meiosis in *Caenorhabditis elegans*. *Genetics* **176**, 2015–2025 (2007).
20. Humphryes, N. et al. The Ecm11–Gmc2 complex promotes synaptonemal complex formation through assembly of transverse filaments in budding yeast. *PLoS Genet.* **9**, e1003194 (2013).
21. Page, S. L. et al. Corona is required for higher-order assembly of transverse filaments into full-length synaptonemal complex in *Drosophila* oocytes. *PLoS Genet.* **4**, e1000194 (2008).
22. Collins, K. A. et al. Corolla is a novel protein that contributes to the architecture of the synaptonemal complex of *Drosophila*. *Genetics* **198**, 219–228 (2014).
23. Ur, S. N. & Corbett, K. D. Architecture and dynamics of meiotic chromosomes. *Annu. Rev. Genet.* **55**, 497–526 (2021).
24. Zhang, F. G., Zhang, R. R. & Gao, J. M. The organization, regulation, and biological functions of the synaptonemal complex. *Asian J. Androl.* **23**, 580–589 (2021).
25. Crichton, J. H. et al. Structural maturation of SYCP1-mediated meiotic chromosome synapsis by SYCE3. *Nat. Struct. Mol. Biol.* **30**, 188–199 (2023).
26. Pyatnitskaya, A., Andreani, J., Guérois, R., De Muyt, A. & Borde, V. The Zip4 protein directly couples meiotic crossover formation to synaptonemal complex assembly. *Genes Dev.* **36**, 53–69 (2022).
27. Dunce, J. M., Salmon, L. J. & Davies, O. R. Structural basis of meiotic chromosome synaptic elongation through hierarchical fibrous assembly of SYCE2–TEX12. *Nat. Struct. Mol. Biol.* **28**, 681–693 (2021).
28. Schild-Prüfert, K. et al. Organization of the synaptonemal complex during meiosis in *Caenorhabditis elegans*. *Genetics* **189**, 411–421 (2011).
29. Cahoon, C. K. et al. Superresolution expansion microscopy reveals the three-dimensional organization of the *Drosophila* synaptonemal complex. *Proc. Natl Acad. Sci. USA* **114**, E6857–E6866 (2017).
30. Klepikova, A. V., Kasianov, A. S., Gerasimov, E. S., Logacheva, M. D. & Penin, A. A. A high resolution map of the *Arabidopsis thaliana* developmental transcriptome based on RNA-seq profiling. *Plant J.* **88**, 1058–1070 (2016).
31. Hurel, A. et al. A cytological approach to studying meiotic recombination and chromosome dynamics in *Arabidopsis thaliana* male meiocytes in three dimensions. *Plant J.* **95**, 385–396 (2018).
32. Jumper, J. et al. Highly accurate protein structure prediction with AlphaFold. *Nature* **596**, 583–589 (2021).
33. Mirdita, M. et al. ColabFold: making protein folding accessible to all. *Nat. Methods* **19**, 679–682 (2022).
34. Lambing, C. et al. *Arabidopsis* PCH2 mediates meiotic chromosome remodeling and maturation of crossovers. *PLoS Genet.* **11**, e1005372 (2015).
35. Lian, Q. et al. The megabase-scale crossover landscape is largely independent of sequence divergence. *Nat. Commun.* **13**, 3828 (2022).
36. Muller, H. J. The mechanisms of crossing-over. *Am. Nat.* **582**, 193–434 (1916).
37. Zickler, D. & Kleckner, N. A few of our favorite things: pairing, the bouquet, crossover interference and evolution of meiosis. *Semin. Cell Dev. Biol.* **54**, 135–148 (2016).
38. Thangavel, G., Hofstatter, P. G., Mercier, R. & Marques, A. Tracing the evolution of the plant meiotic molecular machinery. *Plant Reprod.* **36**, 73–95 (2023).
39. Dunne, O. M. & Davies, O. R. A molecular model for self-assembly of the synaptonemal complex protein SYCE3. *J. Biol. Chem.* **294**, 9260–9275 (2019).
40. Bolcun-Filas, E. et al. SYCE2 is required for synaptonemal complex assembly, double strand break repair, and homologous recombination. *J. Cell Biol.* **176**, 741–747 (2007).
41. Hamer, G. et al. Progression of meiotic recombination requires structural maturation of the central element of the synaptonemal complex. *J. Cell Sci.* **121**, 2445–2451 (2008).
42. Bolcun-Filas, E. et al. Mutation of the mouse Syce1 gene disrupts synapsis and suggests a link between synaptonemal complex structural components and DNA repair. *PLoS Genet.* **5**, e1000393 (2009).
43. Rog, O., Köhler, S. & Dernburg, A. F. The synaptonemal complex has liquid crystalline properties and spatially regulates meiotic recombination factors. *eLife* **6**, e21455 (2017).
44. Leung, W.-K. et al. The synaptonemal complex is assembled by a polySUMOylation-driven feedback mechanism in yeast. *J. Cell Biol.* **211**, 785–793 (2015).
45. Bhagwat, N. R. et al. SUMO is a pervasive regulator of meiosis. *eLife* **10**, e57720 (2021).
46. Rao, H. B. D. P. et al. A SUMO–ubiquitin relay recruits proteasomes to chromosome axes to regulate meiotic recombination. *Science* **355**, 403–407 (2017).
47. Borner, G. V. et al. Crossover/noncrossover differentiation, synaptonemal complex formation, and regulatory surveillance at the leptotene/zygotene transition of meiosis. *Cell* **117**, 29–45 (2004).
48. Smolikov, S. et al. Synapsis-defective mutants reveal a correlation between chromosome conformation and the mode of double-strand break repair during *Caenorhabditis elegans* meiosis. *Genetics* **176**, 2027–2033 (2007).
49. Espagne, E. et al. Sme4 coiled-coil protein mediates synaptonemal complex assembly, recombinosome relocalization, and spindle pole body morphogenesis. *Proc. Natl Acad. Sci. USA* **108**, 10614–10619 (2011).
50. Wang, K., Wang, C., Liu, Q., Liu, W. & Fu, Y. Increasing the genetic recombination frequency by partial loss of function of the synaptonemal complex in rice. *Mol. Plant* **8**, 1295–1298 (2015).
51. Durand, S. et al. Joint control of meiotic crossover patterning by the synaptonemal complex and HEI10 dosage. *Nat. Commun.* **13**, 5999 (2022).
52. Morgan, C. et al. Diffusion-mediated HEI10 coarsening can explain meiotic crossover positioning in *Arabidopsis*. *Nat. Commun.* **12**, 4674 (2021).
53. Fozard, J. A., Morgan, C. & Howard, M. Coarsening dynamics can explain meiotic crossover patterning in both the presence and absence of the synaptonemal complex. *eLife* **12**, e79408 (2023).
54. Zhang, L., Köhler, S., Rillo-Bohn, R. & Dernburg, A. F. A compartmentalized signaling network mediates crossover control in meiosis. *eLife* **7**, e30789 (2018).
55. Zhang, L., Stauffer, W., Zwicker, D. & Dernburg, A. F. Crossover patterning through kinase-regulated condensation and coarsening of recombination nodules. Preprint at *bioRxiv* https://doi.org/10.1101/2021.08.26.457865 (2021).
56. Concordet, J.-P. & Haeussler, M. CRISPOR: intuitive guide selection for CRISPR/Cas9 genome editing experiments and screens. *Nucleic Acids Res.* **46**, W242–W245 (2018).
57. Fauser, F., Schiml, S. & Puchta, H. Both CRISPR/Cas-based nucleases and nickases can be used efficiently for genome engineering in *Arabidopsis thaliana*. *Plant J.* **79**, 348–359 (2014).
58. Morineau, C. et al. Selective gene dosage by CRISPR–Cas9 genome editing in hexaploid *Camelina sativa*. *Plant Biotechnol. J.* **15**, 729–739 (2017).

59. Bechtold, N. & Pelletier, G. in *Arabidopsis Protocols* (eds Martinez-Zapater, J. M. & Salinas, J.) 259–266 (Humana, 1998).
60. Pettersen, E. F. et al. UCSF ChimeraX: structure visualization for researchers, educators, and developers. *Protein Sci.* **30**, 70–82 (2021).
61. Chelysheva, L. A. et al. An easy protocol for studying chromatin and recombination protein dynamics during *Arabidopsis thaliana* meiosis: immunodetection of cohesins, histones and MLH1. *Cytogenet. Genome Res.* **129**, 143–153 (2010).
62. Ross, K. J., Fransz, P. & Jones, G. H. A light microscopic atlas of meiosis in *Arabidopsis thaliana*. *Chromosome Res.* **4**, 507–516 (1996).
63. Vrielynck, N. et al. A DNA topoisomerase VI-like complex initiates meiotic recombination. *Science* **351**, 939–943 (2016).
64. Cromer, L. et al. Centromeric cohesion is protected twice at meiosis, by SHUGOSHINs at anaphase I and by PATRONUS at interkinesis. *Curr. Biol.* **23**, 2090–2099 (2013).
65. Lian, Q., Chen, Y., Chang, F., Fu, Y. & Qi, J. inGAP-family: accurate detection of meiotic recombination loci and causal mutations by filtering out artificial variants due to genome complexities. *Genomics Proteomics Bioinformatics* **20**, 524–535 (2022).
66. Wang, H. et al. The cohesin loader SCC2 contains a PHD finger that is required for meiosis in land plants. *PLoS Genet.* **16**, e1008849 (2020).
67. Fernandes, J. B. et al. FIGL1 and its novel partner FLIP form a conserved complex that regulates homologous recombination. *PLoS Genet.* **14**, e1007317 (2018).
68. Lu, Y., Ran, J.-H., Guo, D.-M., Yang, Z.-Y. & Wang, X.-Q. Phylogeny and divergence times of gymnosperms inferred from single-copy nuclear genes. *PLoS ONE* **9**, e107679 (2014).
69. Bowman, J. L. The liverwort *Marchantia polymorpha*, a model for all ages. *Curr. Top. Dev. Biol.* **147**, 1–32 (2022).

Acknowledgements

We thank L. Iguertsira and Z. Klising for technical help with plasmid construct and fertility characterization, and D. Charif for bioinformatic guidance in the analysis of transcriptomic data. This work has benefited from the support of the Institut Jean-Pierre Bourgin's Plant Observatory technological platforms. This research was funded by ANR (COPATT ANR-20-CE12-0006), by core funding from the Max Planck Society and an Alexander von Humboldt Fellowship to Q.L. The Institut Jean-Pierre Bourgin benefits from the support of Saclay Plant Sciences (ANR-17-EUR-0007).

Author contributions

N.V. produced all the genetic material, analysed the fertility data, produced and analysed the *scep1*$^{-/-}$ plants, produced the SCPE1 and SCEP2 proteins to obtain antibodies, and produced and analysed the immunocytology data at standard resolution. M.P. analysed the localization and distances between SC components, analysed the AlphaFold2 data and produced and analysed the SCEP1 and SCEP2 orthologue data. S.D. produced and analysed the STED immunocytology data. Q.L. analysed the sequencing data and performed the recombination, interference and aneuploidy analyses. A.C., A.H. and J.G. produced the MLH1 and HEI10 immunocytology data. R.G. produced the analysis of the SCEP1–SCEP2 complex with AlphaFold2. M.G. and R.M. contributed to the supervision and analysis of the cytological and genetic data. C.M. led the project, produced the bioinformatic analysis of the transcriptomic data and wrote the paper with input from all co-authors.

Competing interests

The authors declare no competing interests.

Additional information

Extended data is available for this paper at https://doi.org/10.1038/s41477-023-01558-y.

Supplementary information The online version contains supplementary material available at https://doi.org/10.1038/s41477-023-01558-y.

Correspondence and requests for materials should be addressed to Mathilde Grelon or Christine Mézard.

Peer review information *Nature Plants* thanks Ian Henderson and the other, anonymous, reviewer(s) for their contribution to the peer review of this work.

https://doi.org/10.1038/s41477-023-01558-y

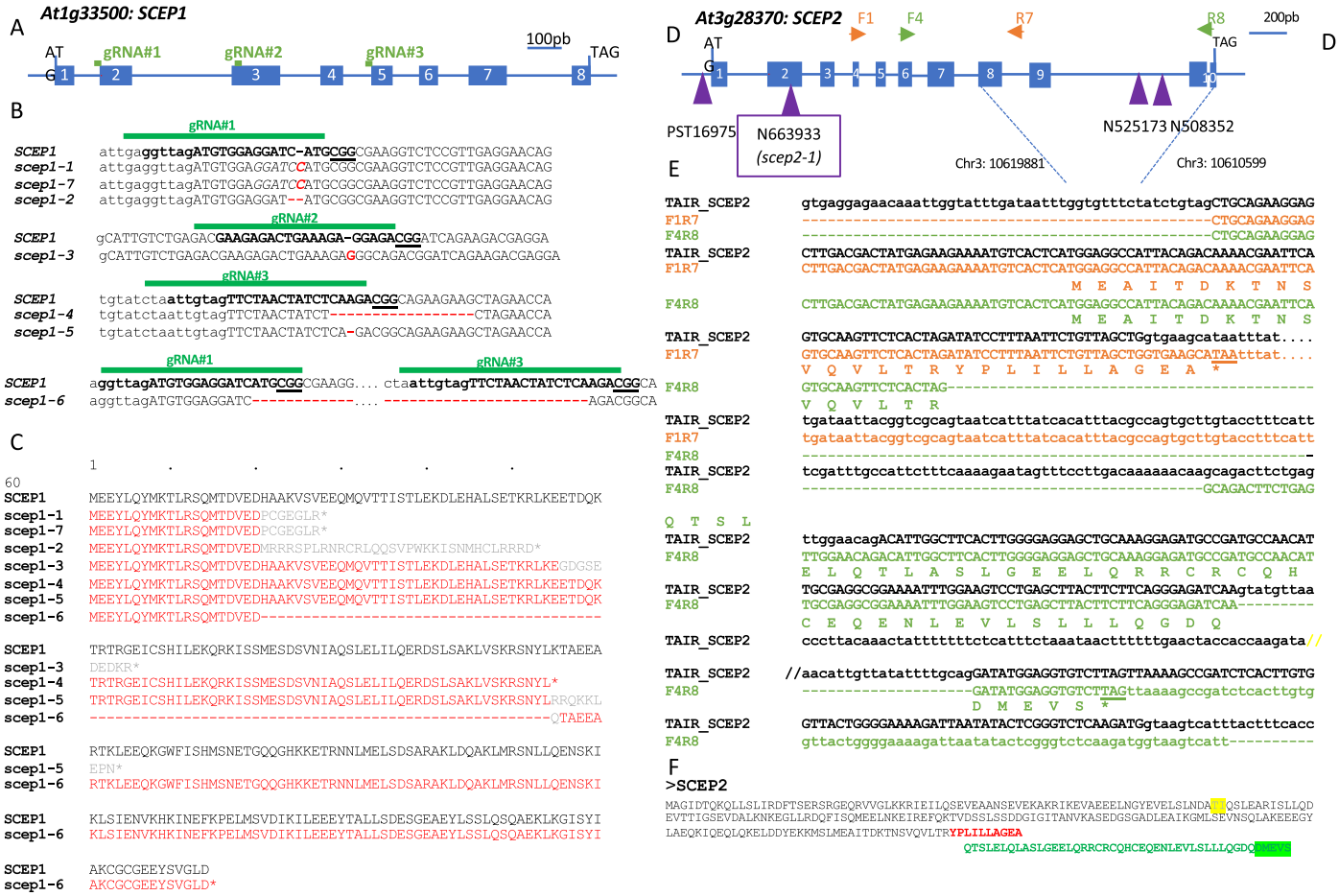

Extended Data Fig. 1 | Description of SCEP1 and SCEP2 protein sequences in the wt and mutants. a. SCEP1 (*AT1G33500*). The exon intron structure of the gene is obtained from the TAIR. The positions of the 3 gRNAs used for CRISPR-Cas9 are shown in green above the gene structure. The positions of the primers used to sequence the 3′ part of the cDNA are shown in black. **b**. DNA sequence of the 7 mutations obtained by CRISPR-Cas9. The sequence of each guide is presented and the PAM is underlined. *scep1-1* in the Columbia background and *scep1-7* in the Landsberg background are identical with an insertion of a C that creates a *Bam*H1 restriction site (italicize). **c**. Protein sequence expected from the mutants obtained by CRISPR-Cas9. Amino acids in red are identical to the wt protein sequence, amino acids in grey differ from the wt due to the frame shift created by the mutations in the open reading frame. * marks the position of the STOP codon. **d**. *SCEP2 (AT3G28370)*. The exon intron structure of the gene is obtained from the TAIR. The positions of the T-DNA insertions are presented below the gene structure with magenta arrows. Among the 4 T-DNA insertions, only the line N663933 (*scep2-1*) exhibits a meiotic phenotype. The positions of the two couple of primers used to sequence the 3′ part of the cDNA are drawn above the gene structure. **e**. The theoretical DNA sequence of the 3′ part of the genomic DNA between the nucleotides 10619881 and 10610599 obtained from the TAIR is written in black with exons in upper case letters. After PCR amplification and sequencing of the cDNA with either the F1-R7 or F4-R8 primers, two cDNA sequences (a short one with the primers F1-R7 and a long one with the primers F4-R8) were obtained producing two isoforms of SCEP2. **f**. The SCEP2 protein sequence with the two isoforms that differ in their 3′ sequence. The position of the N663933 insertion is highlighted in yellow in the coding sequence. The last 5 amino acids removed by the N525173 and N508352 insertions are highlighted in green.

https://doi.org/10.1038/s41477-023-01558-y

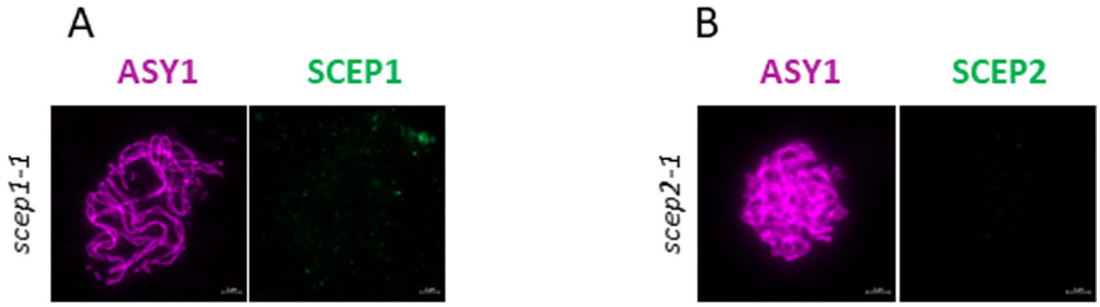

Extended Data Fig. 2 | Test of the specificity of the SCEP1 and SCEP2 antibodies. a. Double immunolocalization ASY1 (Magenta) and SCEP1 (Green) in *scep1-1* male meiocytes. **b**. Double immunolocalization ASY1 (Magenta) and SCEP2 (Green) in *scep2-1* male meiocytes.

https://doi.org/10.1038/s41477-023-01558-y

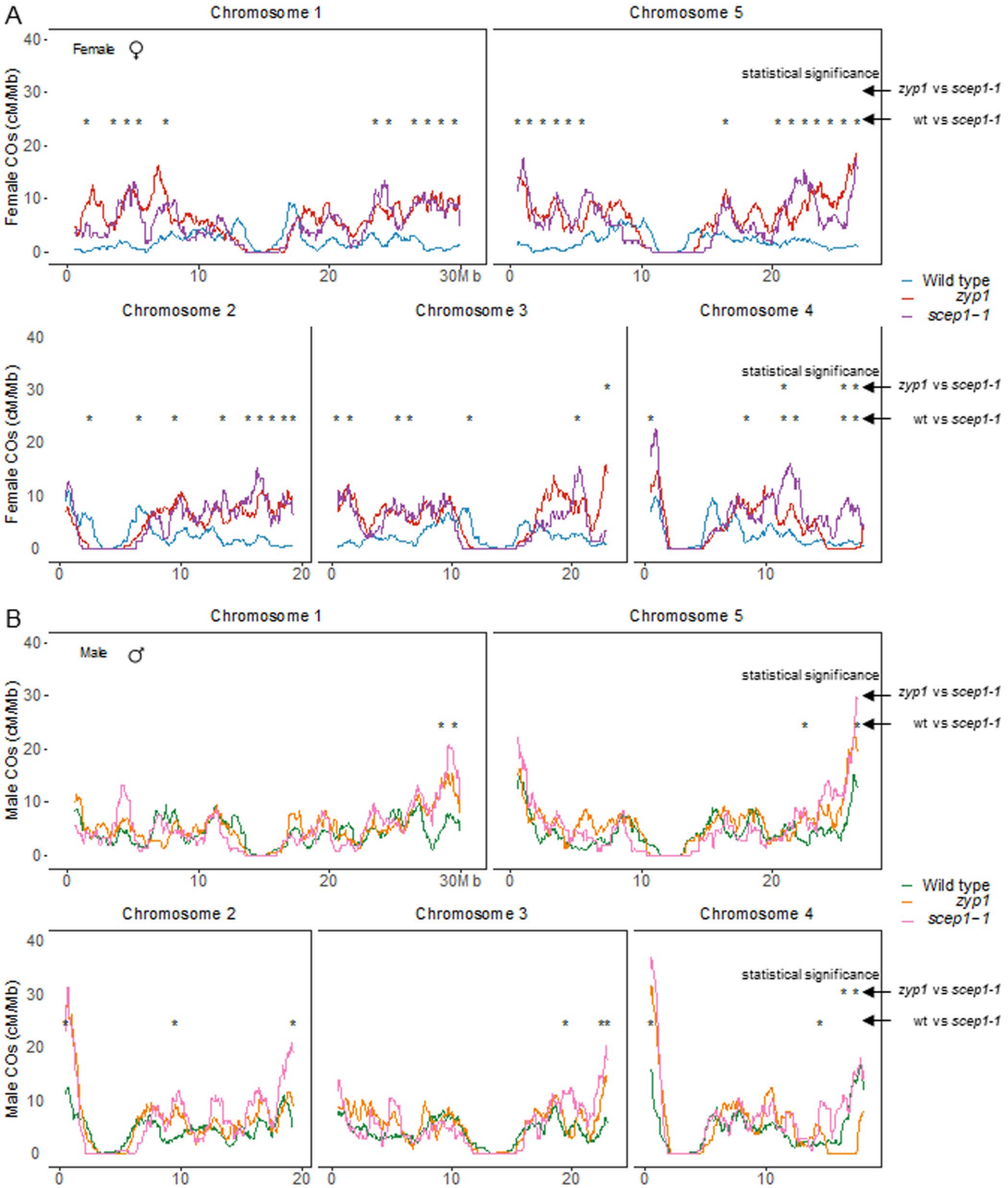

Extended Data Fig. 3 | The distribution of COs along the five chromosomes. The distribution of COs along chromosomes in female (A) and male (B) wild type, *zyp1* and *scep1-1*. The centromere and pericentromeric regions are indicated by gray and blue shading, respectively. Analysis is done with 1-Mb windows and 50-kb sliding steps. For pericentromeric regions and each non-overlapping 1-Mb window along chromosome arms, two-sided Pearson's Chi-squared test was used to examine the difference between wild type and *scep1-1*, *zyp1* and *scep1-1* in female and male populations separately. Windows with p-value (corrected with the FDR method) < 0.05 were marked by stars.

https://doi.org/10.1038/s41477-023-01558-y

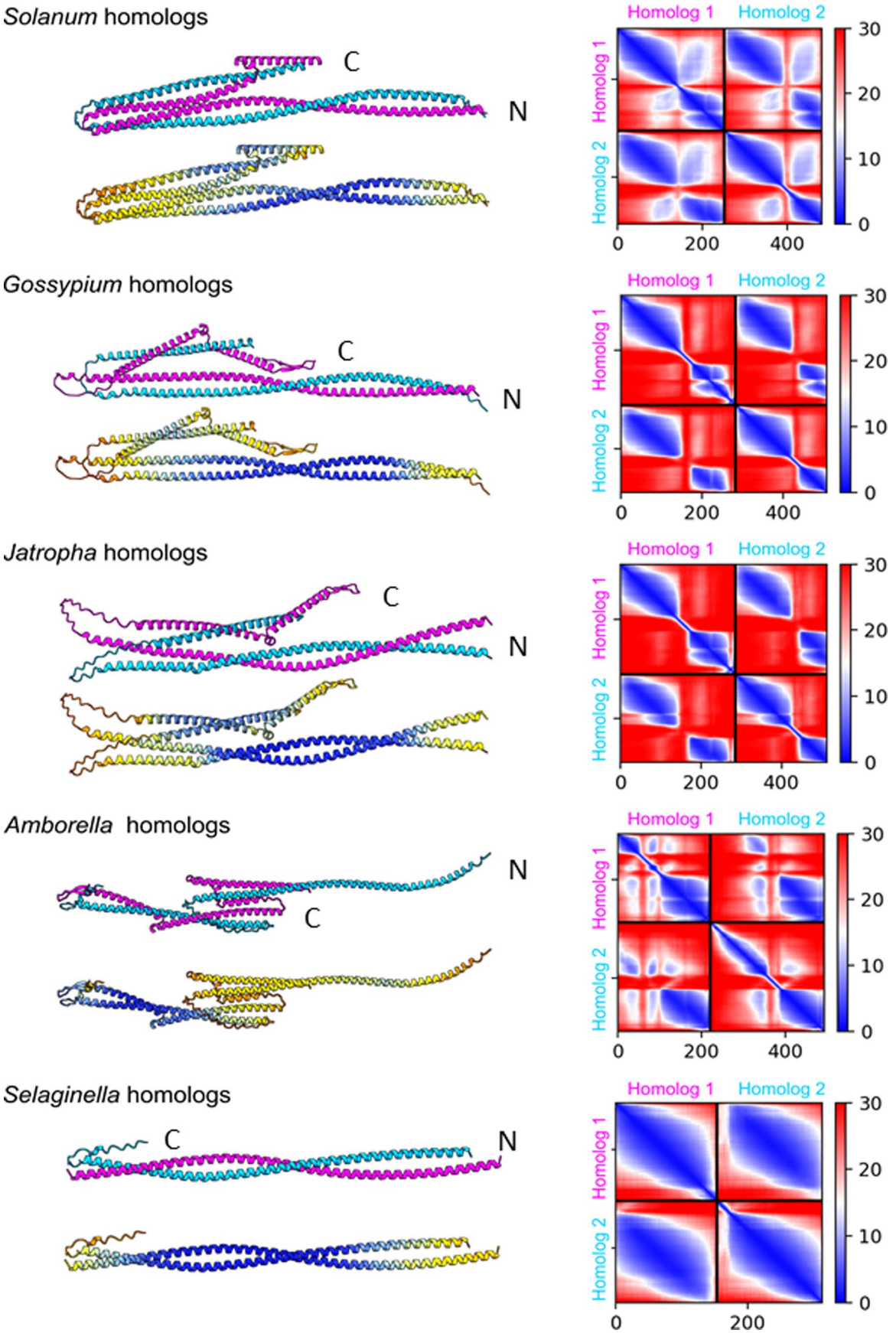

Extended Data Fig. 4 | See next page for caption.

https://doi.org/10.1038/s41477-023-01558-y

Extended Data Fig. 4 | AlphaFold2 prediction of the complex formed by SCEP1 and SCEP2 orthologs in *Selaginella moellendorffii*, *Amborella*, *Jatropha curcas*, *Solanum lycopersicum* and *Gossypium raimondii*. For each species, the top complex represents the SCEP1 homolog in pink and the SCEP2 homolog in blue. The bottom complex is colored by per-residue pLDDT. High pLDDT values indicate strong confidence in the predicted structure, and low values indicate low confidence. Predicted Aligned Error values of the SCEP1-SCEP2 dimer. Low PAE values indicate strong confidence in the relative position of the two amino acids, and high values indicate low confidence.

nature portfolio

Corresponding author(s): Mathilde GRELON, Christine MEZARD

Last updated by author(s): 18/09/2023

Reporting Summary

Nature Portfolio wishes to improve the reproducibility of the work that we publish. This form provides structure for consistency and transparency in reporting. For further information on Nature Portfolio policies, see our Editorial Policies and the Editorial Policy Checklist.

Statistics

For all statistical analyses, confirm that the following items are present in the figure legend, table legend, main text, or Methods section.

n/a	Confirmed	
☐	☒	The exact sample size (*n*) for each experimental group/condition, given as a discrete number and unit of measurement
☐	☒	A statement on whether measurements were taken from distinct samples or whether the same sample was measured repeatedly
☐	☒	The statistical test(s) used AND whether they are one- or two-sided *Only common tests should be described solely by name; describe more complex techniques in the Methods section.*
☒	☐	A description of all covariates tested
☒	☐	A description of any assumptions or corrections, such as tests of normality and adjustment for multiple comparisons
☐	☒	A full description of the statistical parameters including central tendency (e.g. means) or other basic estimates (e.g. regression coefficient) AND variation (e.g. standard deviation) or associated estimates of uncertainty (e.g. confidence intervals)
☐	☒	For null hypothesis testing, the test statistic (e.g. *F*, *t*, *r*) with confidence intervals, effect sizes, degrees of freedom and *P* value noted *Give P values as exact values whenever suitable.*
☒	☐	For Bayesian analysis, information on the choice of priors and Markov chain Monte Carlo settings
☒	☐	For hierarchical and complex designs, identification of the appropriate level for tests and full reporting of outcomes
☒	☐	Estimates of effect sizes (e.g. Cohen's *d*, Pearson's *r*), indicating how they were calculated

Our web collection on statistics for biologists contains articles on many of the points above.

Software and code

Policy information about availability of computer code

Data collection	imageJ for chromosome distance measures. ZEN 2.3 (blue edition) for image acquisition.
Data analysis	R (4.2.2) for distance analyses, differential gene expression analyses, orthologs presentation and yeast-two-hybrid heatmaps. R packages and the versions used: BiocManager (1.30.22); ggplot2 (3.4.2); ggtext (0.1.2); ape (5.7-1); rentrez (1.2.3); tidytree (0.4.5); taxize (0.9.100); tidyverse (2.0.0); rstatix (0.7.2); ggtree (3.8.2); dplyr (1.1.2); ggthemes (4.2.4); stringr (1.5.0); tidyr (1.3.0); ggpubr (0.6.0); treeio (1.24.3); edgeR (3.42.4). Prism-GraphPad (v10.2) for chromosome valency analyses. Genetic map: The raw reads were evaluated for quality by using FastQC version 0.11.9 , and then potential adapter sequences were trimmed and low-quality bases were filtered using Trimmomatic version 0.38 . Then, paired-end reads were aligned to the A. thaliana Col TAIR10 reference genome using Burrows–Wheeler Aligner version 0.7.15-r1140 with default parameters, and those with mapping quality larger than 20 were considered as uniquely mapped and were used in subsequent analysis. inGAP and inGAP-sv were used to identify single-nucleotide polymorphisms (SNPs) and structural variations from resequencing datasets. The Coefficient of Coincidence (CoC) was calculated for CO interference analysis using MADpattern.

For manuscripts utilizing custom algorithms or software that are central to the research but not yet described in published literature, software must be made available to editors and reviewers. We strongly encourage code deposition in a community repository (e.g. GitHub). See the Nature Portfolio guidelines for submitting code & software for further information.

Data

Policy information about availability of data

All manuscripts must include a data availability statement. This statement should provide the following information, where applicable:

- Accession codes, unique identifiers, or web links for publicly available datasets
- A description of any restrictions on data availability
- For clinical datasets or third party data, please ensure that the statement adheres to our policy

Data generated for this manuscript are available E-MTAB-12985 https://www.ebi.ac.uk/biostudies/studies/E-MTAB-12985

Research involving human participants, their data, or biological material

Policy information about studies with human participants or human data. See also policy information about sex, gender (identity/presentation), and sexual orientation and race, ethnicity and racism.

Reporting on sex and gender	NA
Reporting on race, ethnicity, or other socially relevant groupings	NA
Population characteristics	NA
Recruitment	NA
Ethics oversight	NA

Note that full information on the approval of the study protocol must also be provided in the manuscript.

Field-specific reporting

Please select the one below that is the best fit for your research. If you are not sure, read the appropriate sections before making your selection.

☒ Life sciences ☐ Behavioural & social sciences ☐ Ecological, evolutionary & environmental sciences

For a reference copy of the document with all sections, see nature.com/documents/nr-reporting-summary-flat.pdf

Life sciences study design

All studies must disclose on these points even when the disclosure is negative.

Sample size	For valency analysis (Fig 1C) it was decided that at least 50 cells in metaphase I should be observed (including when pooling the different scep1 mutants together). This is usually considered an appropriate, if not in excess, number of cells to conclude on the presence of a meiotic defect in a particular one. Fertility analyses were performed on 10 separate plants for each genotype, with at least ten anthers for each plant. This quantity was determined as it is appropriate to run the statistical tests. For measuring distances between REC8-labelled axial bridges (Fig 2C), 10 independent cells (four for each mutant and two for the wild type) and 25 counts were recorded. This quantity was determined as it is appropriate to run the statistical tests. For measuring distances between observed antibody lines (Fig 4E), measures were done on SCEP1 n=2 cells, 10 measures on each; ZYP1 n=2 cells, 15 measures on each; REC8 n=2 cells 25 measures on each. No difference was observed when independently analyzing the two cells, so these were pooled per antibody. The number of measures is large enough to perform the statistical tests presented. For cytology sample sizes see "Replication" section.
Data exclusions	no data were excluded
Replication	To answer a question of reviewer 2 in the first round of reviews, we added in the revised version "For each genotype, DAPI staining was performed on spreads obtained from pooled anthers from 10 to 20 flowers on one plant for scep1-1, scep1-2, scep1-3, scep1-4, scep1-5, two plants for scep1-6, zyp1-1, scep1-1 scep2-1, scep1-1 zyp1-1, scep2-1 zyp1-1 and 4 plants for wt and scep1-7". This applies both to Figure 1b and Figure 1c. For Figure 2a-b, 3a-d, 4a-d, extended data figure 3a-b, supplementary figures 1a, 2 and 3, immunolabelling was performed on at least 6 slides made with at least 10 anthers coming from at least two to three different plants. It is very hard to report an absolute number as the efficiency of labelling can differ from slides to slides and experiment to experiment. But in all cases the immunolabelling was consistent between the cells observed. In the field, we are not used to give a precise number of cells because the meaning of this number is not helpful.
Randomization	Samples were allocated into experimental groups based on their genotypes, which was determined using PCR amplifications. For image analysis, lines were drawn on random seemingly flat regions.

Blinding	Blinding was not relevant to our study as the group allocation during data collection is based on the genotypes of the plants used to determine relevant phenotypes.

Behavioural & social sciences study design

All studies must disclose on these points even when the disclosure is negative.

Study description	NA
Research sample	NA
Sampling strategy	NA
Data collection	NA
Timing	NA
Data exclusions	NA
Non-participation	NA
Randomization	NA

Ecological, evolutionary & environmental sciences study design

All studies must disclose on these points even when the disclosure is negative.

Study description	Presence or absence of SCEP1, SCEP2 and ZYP1 homologs was determined based on PSI-BLAST results.
Research sample	The presence or absence analysis was performed on a representative set of species.
Sampling strategy	Proteins with an E-value less than 10e-10 and a percent identity greater than 10% were considered potential homologs
Data collection	NCBI PSI-BLASTs against Viridiplantae were used to search for SCEP1 and SCEP2 homologs, with an E-value threshold of 5e-3 and BLOSUM62 matrix.
Timing and spatial scale	PSI-BLASTs were last performed in March 2023 and no difference between previous PSI-BLAST results were found.
Data exclusions	No data matching the criteria described above were excluded.
Reproducibility	This experiment is reproducible given the genomic databases remain unchanged.
Randomization	This is not relevant to our study as no group allocation was performed.
Blinding	This is not relevant to our study as no group allocation was performed.

Did the study involve field work? ☐ Yes ☒ No

Reporting for specific materials, systems and methods

We require information from authors about some types of materials, experimental systems and methods used in many studies. Here, indicate whether each material, system or method listed is relevant to your study. If you are not sure if a list item applies to your research, read the appropriate section before selecting a response.

Materials & experimental systems

n/a	Involved in the study
☐	☒ Antibodies
☒	☐ Eukaryotic cell lines
☒	☐ Palaeontology and archaeology
☒	☐ Animals and other organisms
☒	☐ Clinical data
☒	☐ Dual use research of concern
☐	☒ Plants

Methods

n/a	Involved in the study
☒	☐ ChIP-seq
☒	☐ Flow cytometry
☒	☐ MRI-based neuroimaging

Antibodies

Antibodies used

Polyclonal rabbit anti-SCEP1 or rat anti-SCEP2 antibodies were raised against the full length proteins (see Methods section Production of anti SCEP1, SCEP2 or ZYP1-Cter antibodies) by the Eurogentec company and used at a dilution 1:200 for immunofluorescence. The ZYP1 polyclonal Cter antibody (Lab name: PAK133) was produced against the peptide CEGSLNPYADDPYAFD which is located at the very C-terminus end of the ZYP1 proteins. It was raised in rabbit and affinity purified using the 28-day program of Eurogentec.
For immunostaining, eight primary antibodies were used for both epifluorescence and super resolution microscopy: anti-REC8 raised in rat or in rabbit 65 (dilution 1:250), anti-MLH1 in rabbit (dilution 1/1000), anti-HEI10 in chicken (dilution 1/10000) 51, anti-ASY1 in guinea-pig 31(dilution 1/250), anti-ZYP1 in rat (dilution 1/250), anti-ZYP1-Cter PAK133 in rabbit (dilution 1/200, this study). A list of the secondary antibodies used in thys study is provided in SupTable12
In the material and methods we refer to the article where the antibodies have been tested the first time in mutant cells deprived of the protein concerned and no signal was observed.

Validation

In the material and methods we refer to the article where the antibodies have been tested the first time in mutant cells deprived of the protein concerned and no signal was observed. For SCEP1 and SCEP2 Antibodies we provide in SupFig3 the images of the test of the antibodies against scep1-/- and scep2/- meiocytes